BMC Genomics

RESEARCH

Open Access

Temporal dynamics of chicken host's molecular response against Fowl adenovirus serotype 8b infection via RNA-sequencing

Bahiyah Azli[1], Nur Farhana Salim[1], Mohd Hair-Bejo[1,3], Abdul Rahman Omar[1,3], Norfitriah Mohamed Sohaimi[1,4], Ugwu Chidozie Clifford[3], Nor Asilah Wati Abdul Hamid[5,6] and Nurulfiza Mat Isa[1,2*]

Abstract

Background Fowl adenovirus serotype 8b (FAdV-8b) is the etiological agent of inclusion body hepatitis' outbreaks in chicken farms worldwide and a threat to the poultry industry. The isolation and identification of isolates of this pathogen are abundant, yet the pathogenesis and subsequent molecular mechanism are significantly understudied. Hence, this study aims to identify the differential gene expression profile of specific pathogen-free chicken livers infected with FAdV-8b strain UPMT1901 isolate.

Results The harvested chicken livers were subjected to biological pooling and transcriptomic profiling via RNA-sequencing, according to the days of post-infections (dpi). A total of 21,662 genes were identified in both control and infected groups, enriched in various biological processes and pathways, displaying patterns of disease progressions. The transcriptome analysis results revealed a three-fold reduced pattern of gene regulation with 9146, 7335, and 3800 significant differential expressed genes (DEGs) at 2-, 5-, and 7-dpi (dpi), respectively.

Conclusion These findings elucidate insights on the holistic disease progression of FAdV-8b in liver, from viral incubation and replication at 0–2-dpi, major metabolite hijacking at 3–5-dpi, followed by constant regulation of immune response at 6- and 7-dpi. Based on intensive literature review conducted prior to this study, this study is considered as the first study of the serotype 8b infection pathogenesis at the target organ, providing a better understanding and wide basis of pathogen-host interaction in FAdV-8b in chickens and its progression.

Keywords RNA-Sequencing, Disease progression, Fowl adenovirus, Host response, Transcriptomic, Avian, Temporal, Inclusion body hepatitis

*Correspondence:
Nurulfiza Mat Isa
nurulfiza@upm.edu.my
[1]Laboratory of Vaccine and Biomolecules, Institute of Bioscience, Universiti Putra, putrajaya, Malaysia
[2]Department of Cell and Molecular Biology, Faculty of Biotechnology and Biomolecular Science, Universiti Putra Malaysia, Serdang 43400, Malaysia
[3]Department of Veterinary Pathology and Microbiology, Faculty of Veterinary Medicine, Universiti Putra Malaysia, Serdang 43400, Malaysia
[4]Department of Veterinary Laboratory Diagnostic, Faculty of Veterinary Medicine, Universiti Putra Malaysia, Serdang 43400, Malaysia
[5]Department of Communication Technology and Network, Faculty of Computer Science and Information Technology, Universiti Putra Malaysia, Serdang 43400, Malaysia
[6]Laboratory of Computational Science and Mathematical Physics, Institute of Mathematical Research, Universiti Putra Malaysia, Serdang 43400, Malaysia

Background

Fowl adenovirus (FAdV) outbreaks have led to economic losses in poultry industry across the globe. FAdV is a member of the family of *Adenoviridae* and the genus of *Aviaadenovirus*, elucidated to be a non-enveloped avian-susceptible etiological agent, which consists of double-stranded DNA (dsDNA). This pathogen is classified into five species (i.e. FAdV group A-E), determined by the restriction digest patterns [1] and further grouped among 12 serotypes (FAdV-1 to FAdV-8a and FAdV-8b to 11) depending on the serum cross-neutralization test [2]. FAdV infections in chickens will lead to the manifestation of diseases such as hydropericardium hepatitis syndrome (HHS), inclusion body hepatitis (IBH), avian gizzard erosion (AGE), as well as respiratory diseases such as bronchitis, macro lesions of the kidney [3, 4]. Due to the difference in virulence capacity of serotypes, FAdV strains are profiled to be serotype-unique and predisposed to certain clinical conditions, in which FAdV-C (FAdV-4 and −10) were usually isolates from HHS-positive flocks [5, 6], FAdV-A from AGE-positive groups [7], while FAdV-B, FAdV-D and -E from IBH-positive outbreaks [8–12]. These chickens have shown high mortality and morbidity rates with an abysmal healthy performance of broiler chickens and their progenies. Once infected, the pathogens were reported to cause a sudden onset of mortality of 10–30% rate for FAdV-8b [13, 14], whereas 30–80% rate amongst FAdV-4-infected flocks [5, 15, 16]. Evidence from various epidemiological studies confirmed that IBH occurs mainly in chickens with an age range from three to seven weeks old (i.e. 15–35 days-old chickens), yet also susceptible to age less than one week old (i.e. seven-days old chickens) [17]. The first FAdV-associated outbreak case in Malaysia was technically reported in 2005 [18], resulting in the first isolation and identification of the FAdV-8b strain in Malaysia. To date, there are increasing reports of IBH cases, deeming FAdV-8b as the predominant serotype within the nation's local environment [19–23].

In the last decade, there have been increasing outbreaks of FAdV isolates worldwide, and epidemiological studies, clinical histology, and vaccine production original research have been published yearly [11, 14, 24–26]. Nevertheless, the existing knowledge of FAdV infection mechanisms and transcriptomic profile in a definite host is still underwhelming, with relatively slow progress compared to the other FAdV scopes of study. Liver is the primary target of FAdV-8b, in which hepatic lesions are correlated with three stages of disease progression: [1] incubation (1–3-days post-infection [dpi]), [2] degeneration (4–7-dpi), and [3] convalescence (8–14-dpi). The progression of FAdV-associated diseases was translatable to the clinical, histological, and pathogenicity studies of FAdV isolates. Previously, Steer et al. [27] reported no significant differences between gross lesions of one-day-old specific pathogen free (SPF) Lohmann Select Leghorn chickens during 1- to 3-dpi among groups injected with FAdV-1, FAdV-8b, and FAdV-11. Meanwhile, at 4- to 7-dpi, only chickens from group FAdV-8b and FAdV-11 exhibited significant differences compared to the negative control group. Similarly, mortality of FAdV-4-infected commercial Chinese chicken flocks peaked at 3- to 4-dpi and declined at 9- to 14-dpi, followed by recovery [28]. These findings suggest that, although the identified serotypes differ in virulence, they appear to follow broadly involved in similar stages of disease progression. However, subtle variations in the timing and severity of incubation, degeneration, and convalescence phases indicate that the exact progression patterns between and within serotypes are not yet fully understood. Hence, there is a critical demand to elucidate this research question as insights on the clinical response towards infection may assist the development of vaccines and anti-viral drugs as biological therapies [29–31].

Most pathogens possess the ability to adapt to environmental changes and can naturally adopt alternative strategies to replicate, spread, and survive within the host by evading immune defenses and exploiting host cellular machinery [32–36]. Due to such state-of-the-art on viral infection, the research of host–pathogen interactions has been an evolving field deemed vital to overcome challenges in control, preventive measures, and curing work of the infectious diseases [25, 37]. Previous research studies have proven to be a reliable analysis method for understanding the molecular mechanism, or pathogenesis progression via ChIP-Sequencing [38, 39]. However, the advancement of Next-Generation Sequencing (NGS) imparts opportunities for global transcriptomic studies to skyrocket within the infectious disease research niche which is less-invasive, cost-effective, and time-saving. RNA-Seq has been widely used to study host–pathogen interplay and has been performed on variations of pathogen studies [40]. Numerous transcriptome studies of FAdV provide insights into the infection of FAdV-4 due to its high mortality, despite the low morbidity, yet none were done on the FAdV-8b transcriptome profile [15, 41, 42]. The FAdV-4-related transcriptomes analysis has adopted a pairwise comparison of healthy-vs-treated protocol to elucidate the gene expressions and pathways activities during an infection, mainly which influences the viral invasion, metabolic pathways, and immunosuppression of the infected host. Identification of essential pathways during FAdV infection, such as P13k-Akt and Toll-like receptor signaling pathways, were reported to influence the viral entry [43–46]. In contrast, the Jak-STAT, NOD-like receptor, and cytokine-cytokine receptor signaling pathways regulate the host cell immunosuppression at a later stage of infection for

virions release for further infections [47–49]. Thus, this study aims to elucidate transcriptomic profile of the specific pathogen-free chickens' liver tissues infected with wildtype pathogenic FAdV-8b strain UPMT1901 isolate. The RNA-Seq protocol has provided a comprehensive picture of FAdV infections mechanism on the transcriptomic scale and gained more insights on the virus-host interplay and the pathogenesis of FAdV-8b strains. These create directions and set a valuable basis for further investigation and future FAdV-8b control and preventive measures research.

Methods

Animal trial, sample collection, and ethics statement

All SPF live chickens used in this study were purchased as 9-day-old embryonated chicken eggs from Malaysian Vaccine Pharmaceutical® Sdn. Bhd. (Malaysia). The purchased eggs were let to hatch in a sterilized egg hatcher SIS 1008 AE (Siam Incubator Systems Co., Thailand) with a 37°C, 5% CO_2 setting. During the hatching process, the hatcher racks that locates the eggs were made sure to move 45° automatically, ensuring the heat from the built-in lamps were distributed equally. Additionally, two 1000 mL conical flask filled with sterilised distilled water were put in the hatcher incubator to provide constant humidity inside the hatcher during the process. Once hatched, the healthy 0-day old chicks were housed accordingly to the animal trial design. Twenty-eight 14-days-old SPF live chickens were randomly grouped into two groups, precisely sixteen in Group A (control) and twelve in Group B (infected), respectively. All chickens are sheltered in physically separated experimental rooms at the Animal Research Facility (ARF) of the Faculty of Veterinary Medicine, Universiti Putra Malaysia, under controlled conditions for seven days and strict personnel restrictions for biosecurity and prevention of cross-contamination purposes. To ensure confidence of the control group, chickens from Group A were housed in separate buildings designed specifically to house control groups of animal studies in ARF. These chickens were given an ad libitum access to feed and water intake throughout the trial. Chickens from Group A act as the negative control group, whereas Group B was inoculated with 0.1 mL of $10^{7.79}$ EID50/mL FAdV-8b strain UPMT1901 inoculum subcutaneously [22]. Inoculation of chickens in Group B was done via subcutaneous injection using a 1cc/mL sterilized syringe with a 25G needle (Terumo, Japan). Four chickens from Group A were sacrificed at each 0-, 2-, 5- and 7-dpi, whereas four chickens from Group B were sacrificed at each 2-, 5-, and 7-dpi. All sacrifices were made via cervical dislocation. This animal trial was performed with the approval of the International Animal Care and Use Committee [No: UPM/IACUC/AUP-R065/2020]. Any natural chicken death during the study reduced the scheduled four sacrifices for the nearest time interval, requiring immediate post-mortem examination.

During sampling, the gross lesions of the liver were observed and recorded. Meanwhile, two sets of liver organs were collected; one set was stored in a 1 × Phosphate buffer saline (PBS, 0.1 M, pH 7.4, Life Technologies™, USA) to produce 50% (w/v) solution for viral copy number quantification, and another set was fixed in a 10% Buffer formalin solution for histological examination. The formalin-fixed livers were then subjected to tissue slicing and mounting, followed by staining with haematoxylin and eosin (HE) [50]. The visualization of the stained-glass slides under the Leica DM LB2 light microscope (Leica Camera, German) with × 40 magnification objective. The histological lesion observations were then given a quantitative scoring according to describe in Supplementary Table 1 for each slide, validated by a certified pathologist from Faculty of Veterinary Medicine, UPM. The findings and interpretations were classified and scored based on the severity of the observations, which included the percentage of affected tissue area, cell architecture, and the presence of degenerated cells, sinusoids, and hemorrhages. The classifications included normal, mild, intermediate, or severe states. Another set of liver tissue was also sampled and stored in Solarbio™ RNAwait solution (Solarbio, China) for further RNA extraction and sequencing analysis before the RNA-Seq protocol.

RNA extraction

The harvested liver of SPF chickens in the animal trial were subjected to total tissue RNA extraction via the FavorPrep™ Tissue Total RNA Mini Kit (Favorgen, Taiwan), according to the manufacturer's guidelines. The samples were homogenized with a supplied micro pestle, followed by passing of lysate ten times through a 21G and 25G needle gauge (Terumo, China) in a 1cc/mL syringe (Terumo, China). 60 µL of 1 × Diethyl pyrocarbonate (DEPC)-treated water (1st BASE, Singapore), an elution buffer, was added directly into the center of the column

Table 1 Details of origin of samples for RNA-Sequencing analysis

No	Technical sample name	Number of biological replicates	Description
1	A_ctrl	4	Non-infected liver of 14-days old control SPF live chicken at 0-days post-infection
2	WT_2	4	Infected liver of 14-days old SPF live chickens, at 2-days post-infection
3	WT_5	2	Infected liver of 14-days old SPF live chickens, at 5-days post-infection
4	WT_7	4	Infected liver of 14-days old SPF live chickens, at 7-days post-infection

and incubated at room temperature for 5 min in a standing position. Each column was centrifuged at 15,000 xg for 1 min to elute the RNA. Then, each eluted RNA sample were aliquoted into 50 µL and 10 µL volume for sequencing and RNA integrity analysis, respectively. The extracted total RNA purity and concentration were evaluated via Nanodrop Biospectrophotomer® (Eppendorf, USA), while concentration was via Qubit analysis with RNA Pico chip (Agilent Technologies, USA). In contrast, RNA Integrity Number (RIN) analysis was done via the 2100 Bioanalyzer System (Agilent Technologies, USA). All extracted samples of biological replicates were pooled into one technical replicate (Table 1) and were chosen for RNA-Seq and sent for Next-generation sequencing (NGS) [51]. All extracted samples were outsourced to the Laboratory of Vaccine and Biomolecules 1, Institute of Bioscience, Universiti Putra Malaysia, for quality-checking services before further sequencing analysis. For high-quality sequencing, all the samples were ensured to be at the molecular weight of > 1000 ng, with 280 nm/230 nm wavelength of 2.0 and 260 nm/230 nm wavelength of 2.0–2.2, as well as RIN quality of > 7.

Library construction and sequencing

The construction and sequencing were performed by outsourcing to at NextGene Scientific Sdn. Bhd. (Malaysia). The messenger RNA (mRNA) was purified from the total RNA using poly-T oligo-attached magnetic beads to remove ribosomal RNA (rRNA) using the NEBNext® Poly(A) mRNA Magnetic Isolation Module kit (New England Biolabs, USA). After fragmentation, the purified mRNA was subjected to cDNA library synthesis via TruSeq™ Stranded mRNA kit (Illumina, USA). Post-purification and paired-end repair, the final cDNA fragments were ligated to sequencing adapters and amplified via polymerase chain reaction (PCR) to obtain the final paired-end library raw reads set. The generated cDNA libraries were then subjected to Qubit via the 2100 Bioanalyzer System (Agilent Technologies, USA) by using the DNA-specific chip Agilent DNA 1000 (Agilent Technologies, USA) for size distribution detection and RNA integrity quality checking. The quantified libraries from four groups were subsequently pooled accordingly. Sequencing was conducted via the Illumina platform and Illumina NovaSeq™ 600 System sequencer machine (Illumina, USA) for raw paired-end sequencing files of all four samples in FASTQ format, with different index libraries barcoding of each sample. The sequencing Paired End 150bp (PE150) protocol has been selected for the purpose of this study. The concentration of the final transcriptome raw reads libraries of all samples was determined using the Qubit HS dsDNA kit (Thermo Fisher Scientific, USA) with Qubit via 2100 Bioanalyzer System (Agilent Technologies, USA) for size distribution, concentration, and average size of the raw reads libraries.

Bioinformatics analysis

The quality control checking of raw reads was performed via FastQC [52]. The raw reads produced were subjected to pre-processing to ensure high quality, reliability, and confidence. Only clean reads are subjected to downstream analysis. Upon pre-processing, the raw reads were filtered to remove low-quality reads as follows: (1) removal of adaptor and quality-trimmed short segments of raw reads < 50% and quantity bases < 5 via SeqPrep [53]; (2) sequence with base-quality score < 5 and contains uncertain poly nucleotides (N) constitute base rate of raw reads > 10% via Sickle [54]. The remaining sequence reads were termed "clean reads" and stored in FASTQ format files. Simultaneously, the Phred values > 20% (Q20) and > 30% (Q30) and GC content of the clean reads were mapped and re-evaluated with FastQC, post-cleaning. Only clean reads with high quality and appropriate GC content were further subjected to downstream analyses.

The latest reference genome of *Gallus gallus* GRCg6a (galGal6; female Red jungle fowl; RefSeq No: GCF_000002315.6 [55]) and related gene model annotation files were retrieved online from the NCBI database system. The clean reads library was performed onto reference-mapped against galGal6 reference sequence via HISAT2 v2.0.5 [56], employing the default parameter settings. Next, output of the BAM files was subjected to Stringtie v.1.3.3b [57] for reference-based assembly to generate the contigs library. The gene expression levels were calculated via FeatureCounts v1.5.0-p3 [58] by counting the number of contig reads mapped to each gene in the Gene Transfer Format (GTF) of the galGal6 file. Then, the Fragments Per Kilobase of the transcript sequence per Millions base pairs sequenced (FPKM) of each gene was calculated based on the length of the gene and reads count mapped to the annotated gene to generate a normalized value. Differential analysis was performed onto the cleaned reads using edgeR v.3.22.5 [59], with log2 fold-change were set with parameters of >= 1 and adjusted $P < 0.05$, in which default criteria of |log2 fold-change| > 1 and false discovery rate < 0.05 denoted significant changes in differentially expressed genes (DEGs).

Gene annotations

The corrected gene length bias has been used to query the Differentially expressed genes (DEGs) libraries against Gene Ontology (GO [60]) and Kyoto Encyclopedia of Genes and Genomics (KEGG [61]]), employing clusterProfiler CRAN package [62] to generate enrichment and gene cluster values. All GO terms with adjusted

$P < 0.05$ were considered as terms significantly enriched DEGs. Meanwhile, the KEGG database was utilized to retrieve resources to understand high-level functions and utilities for the biological system, such as the cells, organisms, and ecosystem, from molecular-level information, especially large-scale molecular datasets generated by genome sequencing and other high-throughput experimental technologies. In each GO and KEGG enrichment analysis, only the Top 10 total count, upregulated count, and downregulated DEGs with $P < 0.05$ were tabulated into an input for bar chart visualizations with ggplot2 CRAN R package [63]. The enrichment value of the gene set retrieved from GO and KEGG was performed via the Gene Set Enrichment Analysis (GSEA) tool v4.3.2 [64] to retrieve the fold-change and statistical P-value of the DEGs in pathway-enriched level.

Viral genome copy number quantification

20 mg of each harvested organs were homogenised into a 50% w/v suspension in a 2.0 mL microcentrifuge tube (Eppendorf, Germany) with 1X PBS (Life Technologies™, USA). The suspension was then centrifuged at 650 xg for 10 min. After centrifuging, 200 µL of the supernatant was collected and used as the initial material for the viral genomic DNA extraction of the subsequent process. The viral supernatant harvested for inoculum preparation was performed onto genomic extraction via column-based extraction. InnuPREP® viral DNA/RNA extraction kit (AnalytikJena, Germany) was used according to the manual guide of the manufacturer. The final concentration and purity of the extracted DNA were subjected to quantification via the Nanodrop BioSpectrometer® (Eppendorf, Germany). The ratio 260 nm/280 nm estimates the purity of the extracted DNA, in which an output of 1.8 ~ 2.2 is considered as 'pure' DNA extraction. Only extracted viral DNA with high yield concentration and good purity were further used in the amplification processes.

The viral genome copy number quantification via absolute qPCR were sent for outsourcing service at Apta-NIAGA Sdn. Bhd. (Malaysia). The method applied the generation of standard curve technique. A set of primer and probe consisting of forward primer, reverse primer and a probe were designed via the PrimerQuest® Tool of Integrated DNA Technologies™ (https://sg.idtdna.com/Primerquest/Home/Index) with fibre gene of FAdV-8b UPM04217 (Accession No: KU517714.1 [Mat Isa et al., 2019]) as the reference. Only design set with optimum amplicon length, GC content and appropriate target region of interest were selected for the qPCR protocol (Supplementary Table 2).

The qPCRBIO Probe Mix Separate-ROX kit (PCR Biosystems, UK) was used for the quantification of both viral genome copy number values. Prior to start, the 2X qPCRBIO Probe Mix was briefly vortexed to achieved homogenise solution and proceed normalisation of sample. During sample preparation, the 20 µL final mixture of qCPR in each reaction were prepared as below: 10 µL of 2X qPCRBIO Probe Mix, 0.8 µL of 10 µM forward primer, 0.8 µL of 10 µM reverse primer, 0.4 µL of 10uM designed probe, 0.25 µL of genomic DNA template, and appropriate volume of sterilised deionised water. The amplification was performed with AriaMX Real-Time PCR System thermal cycler (Agilent, USA) and the steps involved are: 95°C for 2 min (initial denaturation), followed by a 40-cycle set with 95°C for 5 secs (denaturation) and 56°C for 20 secs (elongation), and allowed to rest at 12°C to 4°C gradually.

For an absolute quantification qPCR analysis, a standard curve is generated by using a known quantified FAdV DNA concentration as the template with high concentration and good purity. A ten-fold serial dilution of the prepared inoculum were carried out. 900 mL of 1X PBS suspension (Life Technologies™, USA) was supplemented into 2 µL microcentrifuge tubes (Eppendorf, Germany) and labelled from 10^{-1} to 10^{-10} in sequential order at each tube. 100 mL of the freshly prepared viral inoculum was suspended into the first tube with 10^{-1} labelled using a pipette with clean tip. The mixture was then pipetted up and down gently to form a homogenise mixture, before a 100 mL of the well-mixed mixture was pipetted out to insert into the next tube, going down the ten-fold serial dilutions set were prepared and carried out in triplicates per samples. The retrieved Ct values were used to generate a plot of Ct standard curve against the corresponding copy of DNA in each dilution to retrieve the standard curve equation (Supplementary Fig. 1).

Quantitative reverse transcriptase PCR

Seven significant upregulated and downregulated genes retrieved from RNA-Seq analysis were selected for in vitro validation of the reproducibility and repeatability of DEGs in the infected liver tissues of SPF live chickens (Supplementary Table 3). The genes selected for RT-qPCR validation were chosen based on their relevance to key biological processes involved in the infection reported from gene annotation analysis. The total RNA retrieved during extraction of the infected liver was primarily subjected to conversion into cDNA synthesis via Reverse-transcriptase enzyme-based protocol, using the UltraScript™ cDNA Synthesis Kit (PCR Biosystems, UK) following the manufacturer's provided guideline. All reactions were then synthesized in a Bio-RAD® Thermocycler with the temperature setting as follows: 42°C for 30 min (incubation), followed by 85°C for 10 min (Reverse transcriptase enzyme denaturation) and resting at 4°C prior to storage for further application.

Fig. 1 Specific pathogen-free (SPF) live chickens infected with FAdV-8b strain UPMT1901 isolate observed with (**a**) ruffled feathers appearance, (**b**) huddling together, and (**c**) diarrhea presence on the bedding. These clinical symptoms are commonly observed in inclusion body hepatitis (IBH) infected chickens of FAdV-8b

Next, the synthesized cDNA samples were quantified in triplicates via qPCR with the KAPA SYBR® FAST qPCR Master Mix kit (KAPA Biosystems, USA), which utilizes the SYBR Green I dye chemistry [65]. The quantitative amplification was performed onto Bio-RAD CFX96 thermocycler instrument (Bio-RAD, USA) with FAST setting following the described temperature: 95°C for 3 min (enzyme activation), 40 cycles of 95°C for 3 secs (denaturation), 57°C for 30 secs (annealing and extension), followed by 4°C (dissociation). The mRNA levels were calculated with reference to the housekeeping gene Glyceraldehyde-3-phosphate dehydrogenase (GAPDH). The retrieved quantity was performed on percentage knockdown calculation using the ΔΔCq formula [66].

Statistical analysis

All quantitative values from histological liver scorings, qPCR, and qRT-PCR analysis were subjected to a One-way ANOVA statistical test via IBM SPSS Statistics software v26 [67]. Any obtained P value < 0.05 was considered statistically significant between groups for all performed tests followed by the Tukey HSD post-hoc test. However, the retrieved P value specifically from RNA-Seq analysis were adjusted using the Benjamin-Hochberg (BH) calculation, and only the P-adjusted value < 0.05 is considered statistically significant.

Results

Clinical and pathologic features of the FAdV-8b-infected chickens

Throughout the seven-days of observation, no mortality was seen in the control group, while two out of twelve SPF chickens from the infected group inoculated with 0.1 mL of FAdV-8b UPMT1901 died naturally at 4-dpi, indicating a 16.67% mortality rate. However, no death was recorded at 5-dpi onwards. As expected, only chickens from the infected group were reported with low performance in daily routine and lethargic, as well as declined intake of food and water, loose and soiled perineum, severe depression, ruffled feathers, huddling, and little-to-no response during handling, when compared to the control (Fig. 1), throughout the trial. Interestingly, the mentioned decline in clinical symptoms observation was seen in the infected chickens as early as 3- to 4-dpi, severely peaked at 5-dpi, and reduced to mild until 7-dpi.

Next, both groups'gross lesions of the liver of chickens were observed, harvested, and recorded (Fig. 2). No significant gross lesions were observed in the liver of the control group, with dark brick red, smooth and glistening texture throughout the animal trial (Fig. 2a, d, f). However, UPMT1901-infected liver was demonstrated with severe IBH-positive gross lesions of pale-yellow discoloration, swollen and friable texture (Fig. 2b, c, e, g). Interestingly, the observed gross lesions of UPMT1901-infected liver were elucidated to worsen in color and texture as the infection progressed through the days. Besides that, a firm yet yellow-discoloration observed in the liver of dead chickens at 4-dpi of UPMT1901-infected chickens observed (Fig. 2c) may suggest the beginning of detrimental stage of IBH gross lesions in the liver, which primarily effects the color, then the texture of target organ. Then, despite being viable, the chickens at 5-dpi and above were also observed with major IBH gross lesions.

Based on the ANOVA test result, there is a significant difference between the histological lesions of infected liver and the control ($P < 0.001$), especially between dpi of the infected groups ($P < 0.00001$), deeming histological lesions as one of the observations for FAdV-8b disease progression (Table 2). As seen in the histological liver tissue imaging in Fig. 2, the control group of 0-, 2-, 5-, and 7-dpi showed a lack of FAdV-8b histological signs (Fig. 2i, iv, vi). The liver transections also elucidated a normal

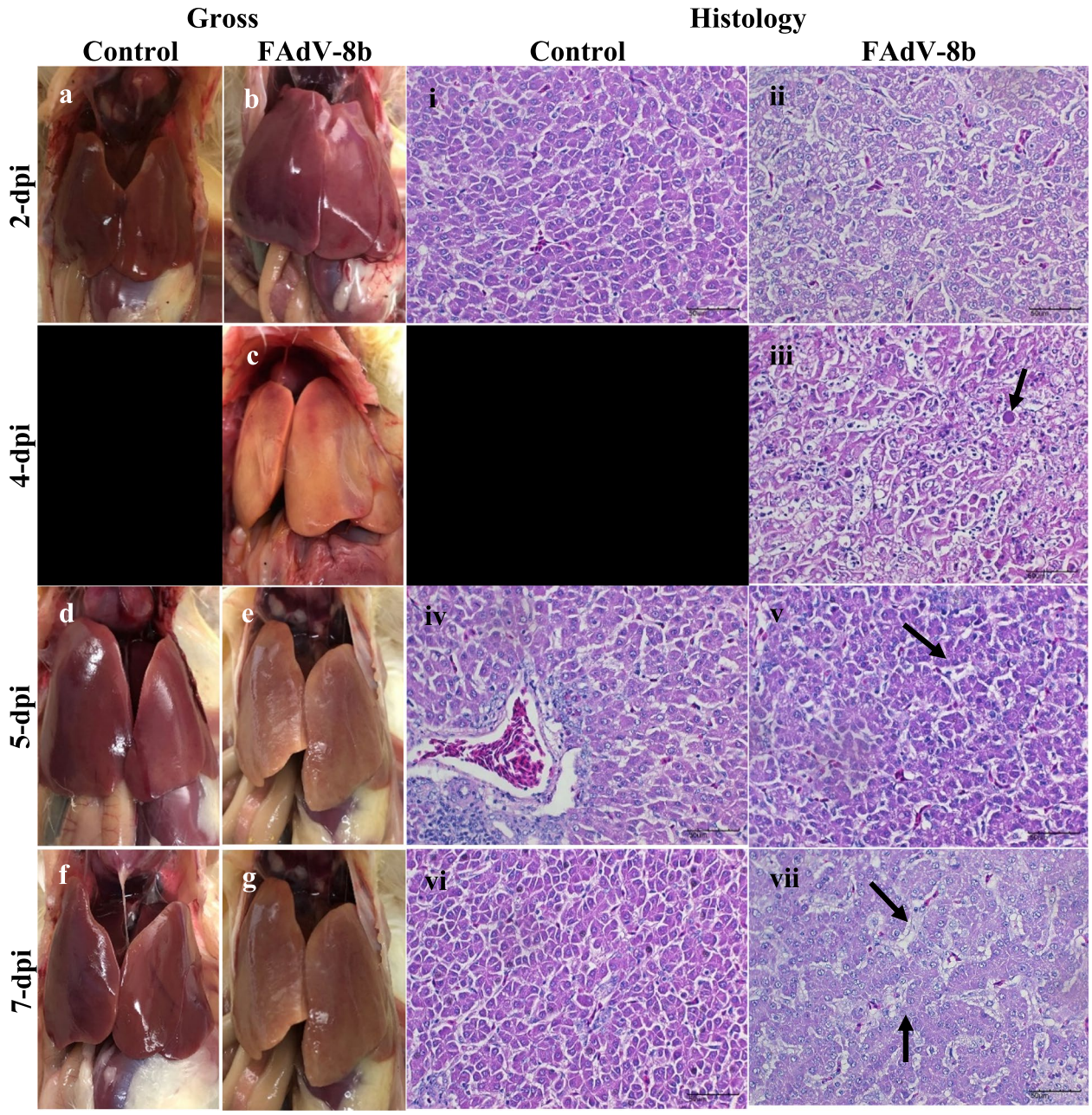

Fig. 2 The pathogenic examination of the infected SPF livers between control and FAdV-8b strain UPMT1901 isolate-infected chickens at 0-, 2-, 4-, 5-, and 7-dpi via gross lesions inspection (a-g) and histological magnification (i-vii) with the scale of 50 µm. Gross liver lesions in infected chickens exhibited pale-yellow discoloration, swelling, and friable texture, worsening with infection progression. Control chicken liver showed normal, dark red livers with smooth and glistening texture. Histological analysis revealed significant intranuclear inclusion bodies (INIBs) in infected livers of the deceased, particularly at 4-dpi, alongside abnormal hepatocyte architecture and porous sinusoids. Infected livers post-5-dpi shows abnormal cell architecture and porous sinusoids, despite no mortality. Meanwhile, control chickens exhibited normal liver architecture without pathological signs. Images for the Control group at 4-dpi (both gross and histology) are missing due to the chickens' death prior to the scheduled necropsy date

Table 2 Histological lesion scoring of liver of specific-pathogen free live chickens infected with FAdV-8b UPM T1901

Group	Days post-infection, dpi				
	0	2	4	5	7
Control	0 ± 0	0 ± 0	-	0 ± 0	0 ± 0
Infected	0 ± 0	1 ± 0	2 ± 0	1.5 ± 0.5	2 ± 0

Table 3 Virus copy number liver of specific-pathogen free live chickens infected with FAdV-8b UPM T1901 *ND = Not detected

Group	Days post-infection, dpi			
	0	2	5	7
Control	ND	ND	ND	ND
Infected	ND	$2.32\times10^{9}\pm2.87\times10^{9}$	$4.20\times10^{9}\pm2.72\times10^{9}$	$1.28\times10^{6}\pm1.86\times10^{6}$

Table 4 Raw and clean reads statistics for RNA-Sequencing analysis

Sample	Total raw reads	Total raw reads bases	Total clean reads	Total clean reads bases	Total error rates, %	Q20	Q30	GC, %
A_ctrl	116,070,612	17.41G	112,000,000	16.83G	0.02	97.97	94.5	50.54
WT_2	51,136,814	17.48G	109,000,000	16.36G	0.03	96.99	92.96	55.23
WT_5	48,718,058	17.6G	112,000,000	16.79G	0.03	97.48	93.66	53.33
WT_7	46,292,166	6.94G	45,904,594	6.89G	0.03	97.52	93.39	50.16

cell architecture of growth and development, whereas the UPMT1901-infected chickens' histological analyses indicated the presence of significantly huge intranuclear inclusion bodies (INIBs) in the liver tissues of the deceased chickens' livers (Fig. 2iii). Likewise, hepatocyte tissues of 7-dpi infected with UPMT1901 were observed with abnormal cell architecture, porous sinusoids with no congestion of hemorrhage, nevertheless with an unclear observation of INIBs (Fig. 2vii). The definite evidence by both gross and histological findings, the post-mortem examination of the infected liver from deceased SPF chickens at 4-dpi has confirmed that the cause of death was FAdV-8b infection.

The analysis of viral genome copy numbers in liver tissues of SPF chickens, as shown in Table 3, provides valuable insights into the viral dynamics of UPM T1901 strains over the 7-day trial. Group A (control) showed no detectable viral presence at any timepoint, confirming the absence of viral infection under control conditions. Meanwhile, the infected group demonstrated consistently higher viral loads compared to control, starting at 2.32×10^{9} at 2-dpi and dropping to 1.28×10^{6} by 7-dpi. This pattern highlights the strong replication capacity of UPM T1901. Also, it elucidates that UPM T1901 replication peaks at 5-dpi, prior to viral clearance at 7-dpi, which may suggest UPM T1901 infection in live host occurred robustly complex. The ANOVA analysis showed a significant effect of treatment (ANOVA, P value = 0.033), indicating that viral load differences between groups are statistically significant.

RNA-sequencing and read assembly

Only four total RNA extracted samples were subjected to sequencing, specifically A_ctrl, WT_2, WT_5, and WT_7. To ensure holistic expressions during the RNA-Seq analysis, the FAdV-8b UPMT1901-infected livers harvested from 14-day-old SPF alive chickens were pooled into one sample per dpi (WT_2, WT_5, and WT_7) [51, 68]. Only three-time points, specifically 2-, 5-, and 7-dpi, were chosen to capture the whole disease period and examine the severity of the disease on the transcriptome level. The raw reads consist of paired-end libraries with a length of 150 base pairs (bp) per reads, with reported < 0.05% error rate, > 96% Q20, > 92% Q30, and GC content of 50.16–55.23% (Table 4). The FastQC reported that approximately 45–109 million clean reads passed the per base sequence quality, per tile sequence quality, per sequence quality scores, per base N content and adapter content. These reports of clean reads statistics permit the progression to the next assembly stage.

Then, the retrieved clean reads from post- and pre-processing were mapped via reference-based alignment against the latest *Gallus gallus* RefSeq annotation, galGal6 (RefSeq No. GCF_000002315.5). The total reads mapped against the reference genome were reported with 87.65–94.11% (Table 5), suggesting most of the clean paired-end reads were successfully mapped against galGal6. Meanwhile, the relatively similar values between mapped clean reads form Read 1 and Read 2 with ~ 1:1 ratio, respective to each sample, indicated the high-quality performance of technical sequencing and the pre-processing process of reads. Upon aligning and mapping against galGal6 via HISAT2 tool, the contigs that covered the exon, intron, and intergenic annotated regions were also analyzed. Accordingly, all samples from all groups show similar mapping statistics percentages of exons, introns, and intergenic reads, approximately > 94.19%, > 1.7%, and > 2.7%, respectively, seen between all samples (Table 6). These pre-processing reports indicated that the read mapping protocols were performed efficiently, successfully eliminating reference-based mapping biases between samples. Exon-mapped read percentage is expected to be tabulated as the highest mapped regions representing the coding regions of genome and indicating galGal6 reference genome as a well-annotated sequence, specifically for transcriptomic studies of SPF chicken breed.

Gene profile statistics

Post-reference-based mapping, the gene count and FPKM values were retrieved by subjecting the clean aligned reads to the featureCount CRAN R package. As seen in

Table 5 Reference-based mapping statistics of clean reads against galGal6 reference genome for RNA-Sequencing analysis

Sample	Total reads	Total mapped reads	Total unique mapped reads	Total multi-mapped reads	Total mapped reads of 1	Total mapped reads of 2	Total mapped reads in positive-strand	Total mapped reads in negative-strand	Total mapped reads in splice regions
A_ctrl	112,182,796	105,574,498 (94.11%)	101,864,763 (90.8%)	3,709,735 (3.31%)	51,007,003 (45.47%)	50,857,760 (45.33%)	50,986,518 (45.45%)	50,878,245 (45.35%)	49,353,139 (43.99%)
WT_2	109,086,338	95,617,728 (87.65%)	91,812,049 (84.16%)	3,805,679 (3.49%)	45,999,220 (42.17%)	45,812,829 (42.0%)	46,207,046 (42.36%)	45,605,003 (41.81%)	34,336,545 (31.48%)
WT_5	111,947,052	101,681,557 (90.83%)	97,893,767 (87.45%)	3,787,790 (3.38%)	49,103,138 (43.86%)	48,790,629 (43.58%)	49,114,279 (43.87%)	48,779,488 (43.57%)	44,207,113 (39.49%)
WT_7	45,904,594	43,047,845 (93.78%)	40,777,310 (88.83%)	2,270,535 (4.95%)	20,468,022 (44.59%)	20,309,288 (44.24%)	20,395,152 (44.43%)	20,382,158 (44.4%)	19,164,466 (41.75%)

Table 7, all samples have relatively similar gene count and FPKM values, with WT_2 as the lowest and A_ctrl the highest, 16,539 and 18,094 counts, respectively. Meanwhile, the FPKM of gene per treatment is 18,094 in control and 19,484 in UPMT1901-infected groups, depicting samples of liver infected with UPMT1901 has a higher gene profile compared to the control. Furthermore, more minor gene FPKM per group at sample WT_2, WT_5, and WT_7 potentially suggesting a robust gene expression in infected liver compared to the control.

During the annotation, 20,489 genes were reported to be identified between all four groups. However, as seen in Fig. 3a, only 8814 genes were commonly shared, elucidating potential conserved housekeeping genes vital for the liver's cell activities regardless of the presence of FAdV-8b nor progressions of the disease. Meanwhile, WT_2 was seen with the highest unique genes of 1061, whereas WT_7 has the lowest unique genes of 182 (Fig. 3b), probably indicating a reduced gene expression. Nevertheless, it is important to highlight the relatively comparable number of identified genes between A_ctrl (342) and WT_5 (345). This similarity may reflect a distinct gene expression profile involved in regulating cellular activities that facilitate pathogen survival. Interestingly, 10,151 genes were commonly expressed in control and infected groups (Fig. 3c), indicating that up to 77.9% of genes might be involved in normal cellular processes activities. Meanwhile, 2546 genes are unique to FAdV-8b infection, and 342 genes are unique to healthy liver tissues, which are potentially the genes that are upregulated and downregulated upon an FAdV-8b infection.

21,662 genes were identified among all four control and infected samples, whereas only 19,484/21662 (89.95%) genes were reported in FAdV-8b infected groups (Fig. 3b, c). By referring to the post-normalization of genes with FPKM, liver infected with FAdV-8b had shown smaller FPKM than the control with a slight difference of around ~ 1000–2000 genes, potentially indicating lesser genes are expressed in an FAdV-8b-infected liver. Nevertheless, the sum of genes FPKM between all three-infection timepoints identified gene in the FAdV-8b-infected liver is 1390 genes higher than the control liver, further hypothesizing that FAdV-8b different time points of infection expressed different genes, summing up into higher gene FPKM per treatment. When comparison was performed against control, WT_2, WT_5, and WT_7 shared 8814 (67.6%) genes, potentially involved as housekeeping genes to maintain cellular activities, whereas 19.5% (2546) genes were uniquely expressed in FAdV-8b infections only, deeming FAdV-8b infection to be specific and pathogenic.

Table 6 Region profile of clean reads retrieved from reference-based mapping against galGal6 reference genome for RNA-Sequencing analysis

Sample	Exon	Intron	Intergenic
A_ctrl	14,926,573,205 (94.55%)	431,571,659 (2.74%)	428,914,810 (2.72%)
WT_2	13,448,059,229 (94.19%)	279,403,779 (1.97%)	550,483,575 (3.86%)
WT_5	14,370,019,446 (94.59%)	272,050,339 (1.79%)	549,864,318 (3.62%)
WT_7	6,085,301,081 (94.69%)	138,811,354 (2.16%)	202,460,973 (3.15%)

Table 7 The tabulated gene count and FPKM of all four transcriptome samples

Sample	Description	Gene count	Gene FPKM	Gene FPKM per group	Gene FPKM per treatment
A_ctrl	Control	18,094	18,094	18,094	18,094
WT_2	FAdV-8b UPMT1901-infected	16,539	16,539	16,539	19,484
WT_5		17,893	17,893	17,893	
WT_7		17,668	17,668	17,668	

Identification of differentially expressed genes

The external RNA Controls Consortium (ERCC) spike-ins for further RNA-Seq analysis were performed via employment of the control-vs-treated analysis. After the clean reads of all transcriptomes were quantified, the expression levels of each identified gene were subjected to the edgeR tool. Each dot in the volcano plot represents DEGs, with red representing the upregulated, green representing the downregulated, and blue representing the no expression difference. The plots in Fig. 4a, b, and c displayed narrow, yet tall dots distribution of the DEGs in UPMT1901-infected liver at all time points, suggesting infected groups to have robust gene expression profiles throughout the disease progression of IBH.

Upon comparison with A_ctrl, 9146 DEGs were reported in WT_2, 7335 DEGs in WT_5, and 3800 DEGs in WT_7, reporting WT_2vsA_ctrl with the highest DEGs, followed by WT_5vsA_ctrl and WT_7vsA_ctrl (Table 6). The comparison of samples suggests relatively three-times fold reduction in gene expression activities throughout IBH disease progression, highlighting the most robust time points post-infection being 2-dpi. Among all pairwise comparisons, only WT_7vsA_ctrl was reported with lower downregulated DEGs, whereas other pairwise comparison groups had higher upregulated DEGs than the downregulated DEGs (Fig. 5). The progressive reduction in DEGs over time suggests a shift back toward a gene expression profile more similar to the baseline.

Next, the heat map of Fig. 6 was generated from DEGs of all three pairwise comparison groups to visualize the global temporal dynamic and progression of gene expression changes. WT_2vsA_ctrl and WT_5vsA_ctrl were positioned in similar dendrogram branch, demonstrating that expression pathways in infected liver at 2-dpi having a similar profile with liver infected with UPMT1901 at 5-dpi, indicating an early response cluster. Meanwhile, WT_7vsA_ctrl outer branching indicates a substantial change of gene expressions pattern profile by 7-dpi compared to the others. Interestingly, the generated DEG heat map Fig. 6 elucidates the overall gene expression patterns between infection time points, highlighting the similarity between genes expressed in 2- and 5-dpi. It is suspected that both 2- and 5-dpi and 5- and 7-dpi of an FAdV-8b infection might overlap with some vital processes, but not 2- and 7-dpi.

GO enrichment analyses of DEGs

These GO terms provide detailed information on the gene and its gene products upon translation in a narrow-to-wide hierarchical structure, from specific to general terms, in which BP describes a series of events or set of dynamic molecular activities organized into pathways or more extensive processes, while MF focuses on the biochemical activity of the gene product itself. 283, 346, and 200 BP terms, as well as 23, 39, and 25 MF terms, were significantly enriched in WT_2vsA_ctrl, WT_5vsA_ctrl, and WT_7vsA_ctrl, respectively.

In Fig. 7, WT_2vsA_ctrl's Top 3 highest DEGs counts in the cell communication, signaling, and organic cyclic compound biosynthesis process, while WT_5vsA_ctrl, signaling, signal transduction, and system development are the BP terms with the highest DEGs counts. Then, the Top 3 BP terms with the highest DEGs are multicellular organism development, animal organ development, and small molecule metabolic process in WT_7vsA_ctrl. The reduced total counts of DEGs enriched from 2- to 7-dpi highlighted a decline in the robustness of gene expression post-infection in infected tissues, further proposing the notion that the disease is progressing towards normal control cellular activity profile.

Next, in Fig. 8, in WT_2vsA_ctrl's Top 3 MF terms with the highest DEGs are molecular function regulator, DNA binding transcription factor activity, and signaling receptor binding, while the highest DEGs MF terms in WT_5vsA_ctrl involved metal ion binding, cation binding, and signaling receptor binding. In WT_7vsA_ctrl, the Top 3 MF terms with the highest DEGs counts are

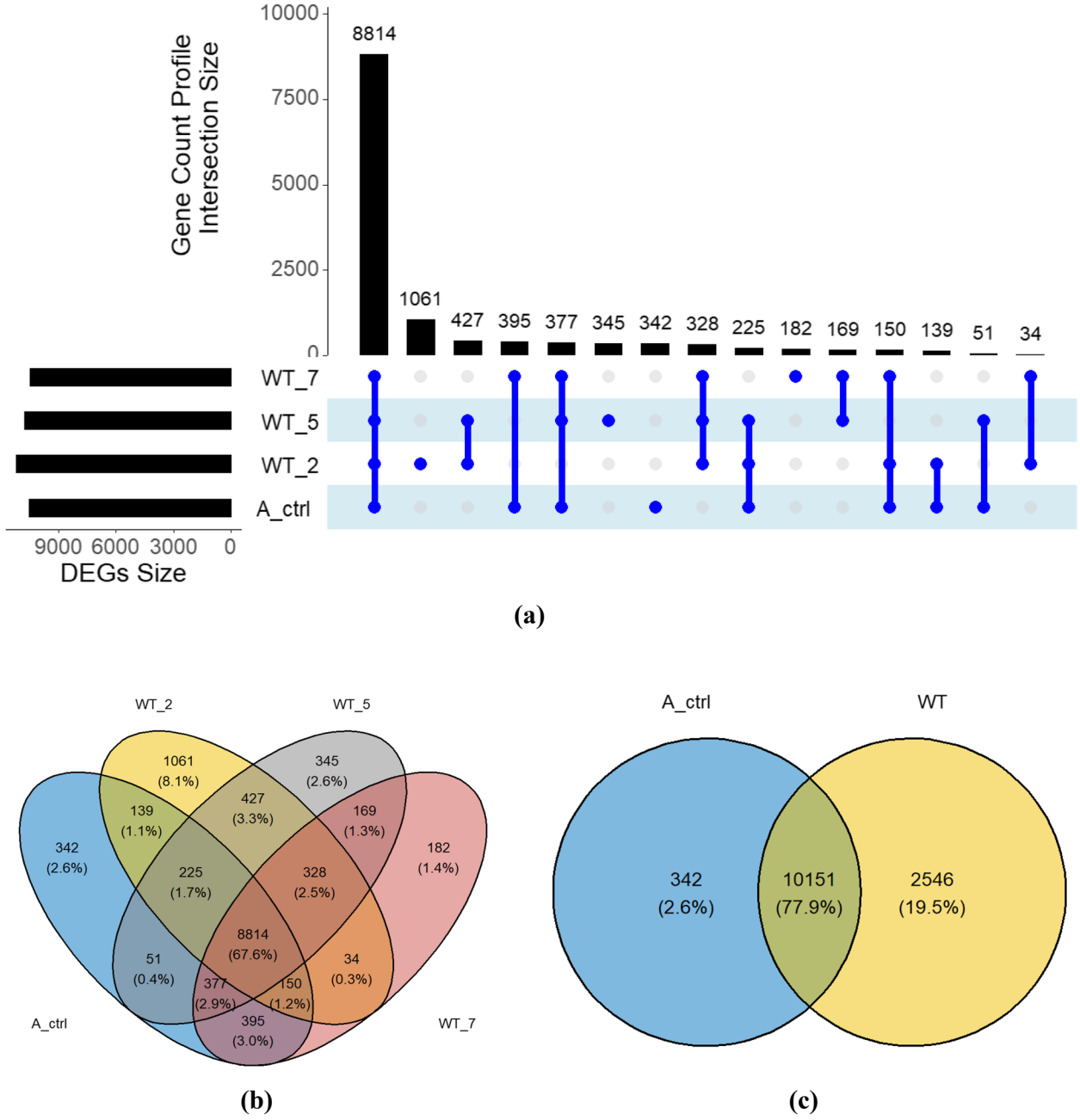

Fig. 3 **a** UpSet plot and **b**,**c** Venn diagram of several genes shared and uniquely expressed within A_ctrl, WT_2, WT_5, and WT_7, as well as between control and FAdV-8b strain UPMT1901-infected cells

cation binding, receptor regulatory activity, and receptor ligand activity. These findings proposed that viral replication processes are uniquely present at 2-dpi, while membrane protein-related processes are abundant at 7-dpi.

KEGG pathway enrichment analyses of DEGs

KEGG pathway analysis was performed to characterize the functional effects of gene expressions between time points upon infections of FAdV-8b strain UPMT1901 isolate. 27, 48, and 29 pathways were significantly reported to be enriched in each time point, respectively. In WT_2vsA_ctrl, the KEGG terms with the highest DEGs counts are neuroactive ligand-receptor interaction, cytokine-cytokine receptor interaction, and influenza A. In WT_5vsA_ctrl, the Top 3 terms with the highest DEGs counts are MAPK signaling pathway, neuroactive ligand-receptor interaction, and cytokine-cytokine receptor interaction, while in WT_7vsA_ctrl, the neuroactive ligand-receptor interaction, cytokine-cytokine receptor interaction, and cell adhesion molecules are the Top 3

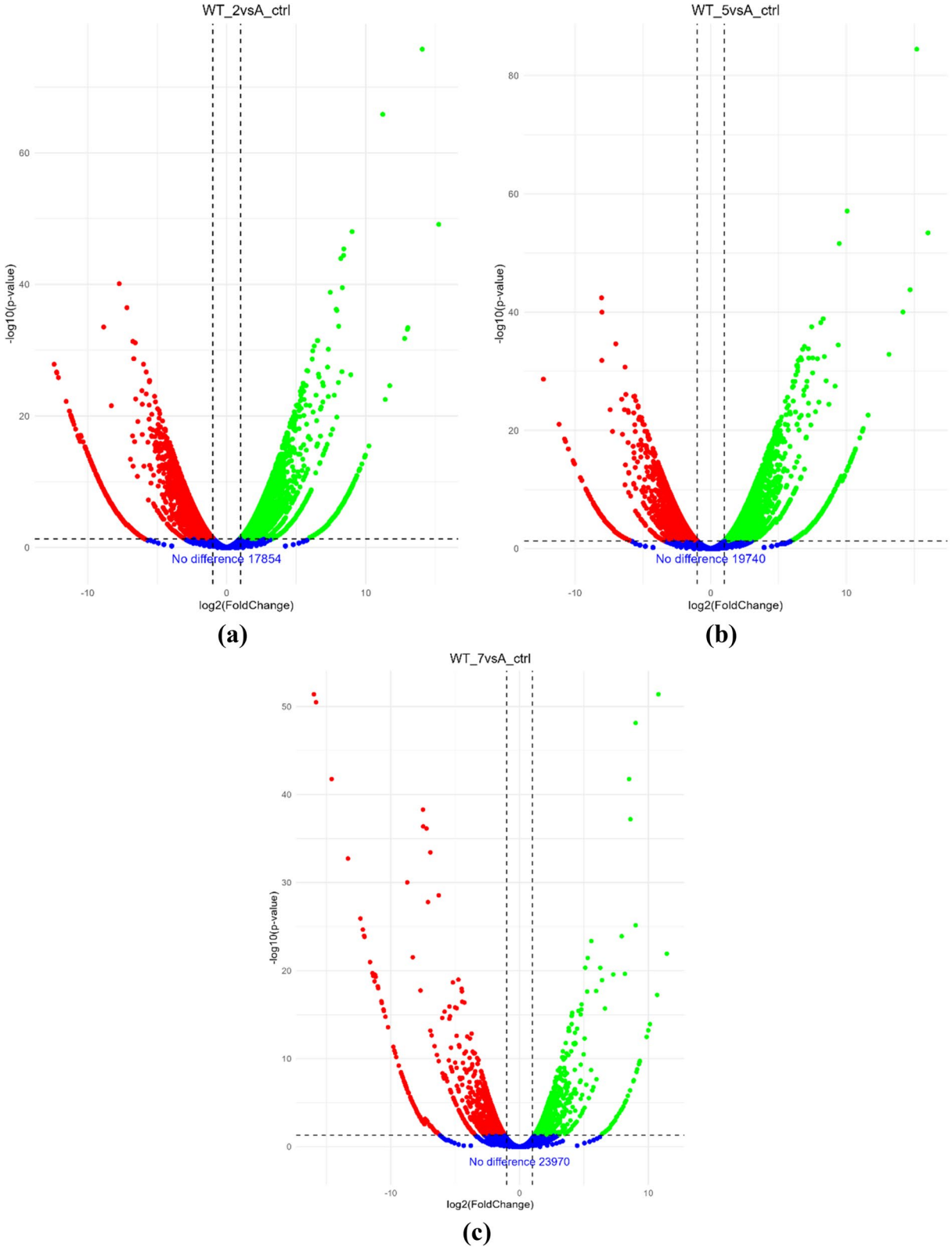

Fig. 4 Volcano plots of the overall distributions of Differentially expressed genes (DEGs) between (**a**) WT_2, (**b**) WT_5, and (**c**) WT_7 against A_ctrl

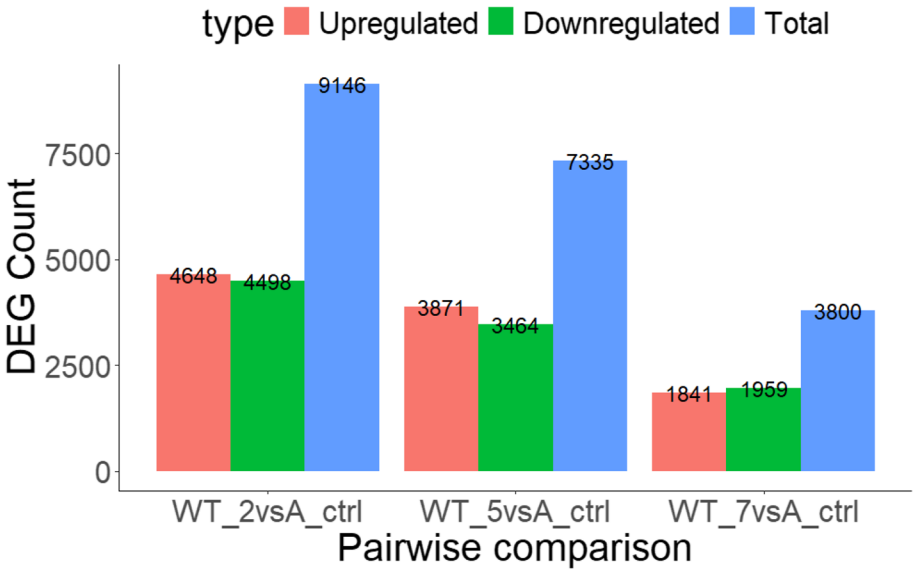

Fig. 5 Bar chart figure DEG gene counts of all upregulated and downregulated Differentially expressed genes from pairwise comparison of WT_2vsA_ctrl, WT_5vsA_ctrl, and WT_7vsA_ctrl

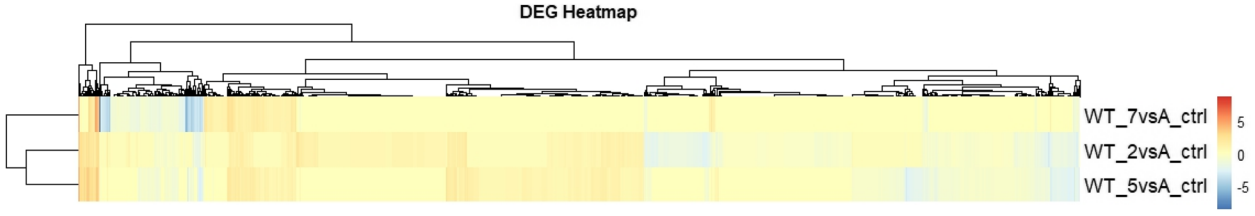

Fig. 6 Summary heat map of Differentially expressed genes profile from pairwise comparison of WT_2vsA_ctrl, WT_5vsA_ctrl, and WT_7vsA_ctrl. Fig. 7. Bar chart of Gene ontology term biological process (BP) classes with upregulated and downregulated Differentially expressed gene counts identified in WT_2vsA_ctrl, WT_5vsA_ctrl, and WT_7vsA_ctrl

terms with the highest DEGs counts. Figure 9 depicted that WT_5vsA_ctrl pathways house higher values of DEGs compared to other time points, altering the most cellular processes for FAdV-8b infection. Also, interestingly, FAdV-8b triggers similar immune and stress response as seen in other viral infections such as Influeza A and Herpes simplex virus 1.

Validation of RNA-sequencing results

RT-qPCR was performed to detect the expression of one metabolite regulator gene (phosphoenolpyruvate carboxykinase 1 [PCK1]), one cytoskeletal-related gene (actin beta [ACTB]), and four inflammatory response genes (C–C motif chemokine ligand 4 [CCL4], suppressor of cytokine signaling 1 [SOCS1], BCL2 like 1 [BCL2L1], and interleukin 18 receptors 1 [IL18R1]), in all three-time points. Six significant differentially expressed genes identified in silico RNA-Seq analysis were chosen and selected as target genes to be validated via comparison with in vitro RT-qPCR. As observed in Fig. 10, the changed of biological patterns of gene expressions are consistent between both in silico and in vitro protocols at all three-time points. Despite the slight differences in values between log2 fold change of in vitro and the relative expressions level of in silico, the pattern of the general expressions was largely consistent, further supporting the reliability of our RNA-Seq data.

Discussion

FAdV infection has been significant veterinary medicine and poultry industry concerns for several years, with increasing reports of IBH-positive outbreak cases in poultry farmhouses [11]. However, limited understanding of the gene functions involved in the pathogenesis and mortality of FAdV-8b infection, particularly in IBH in chickens, hinders progress toward effective control and prevention strategies. The research on molecular mechanism studies of FAdV-8b infections remains understudied. Hence, employing RNA-Seq technology is an essential step in annotating the pathogenesis of IBH among chickens by elucidating each of the stages and mechanisms of infections.

In this project, the relationship between the clinical signs, gross lesions, and histological findings in FAdV-8b

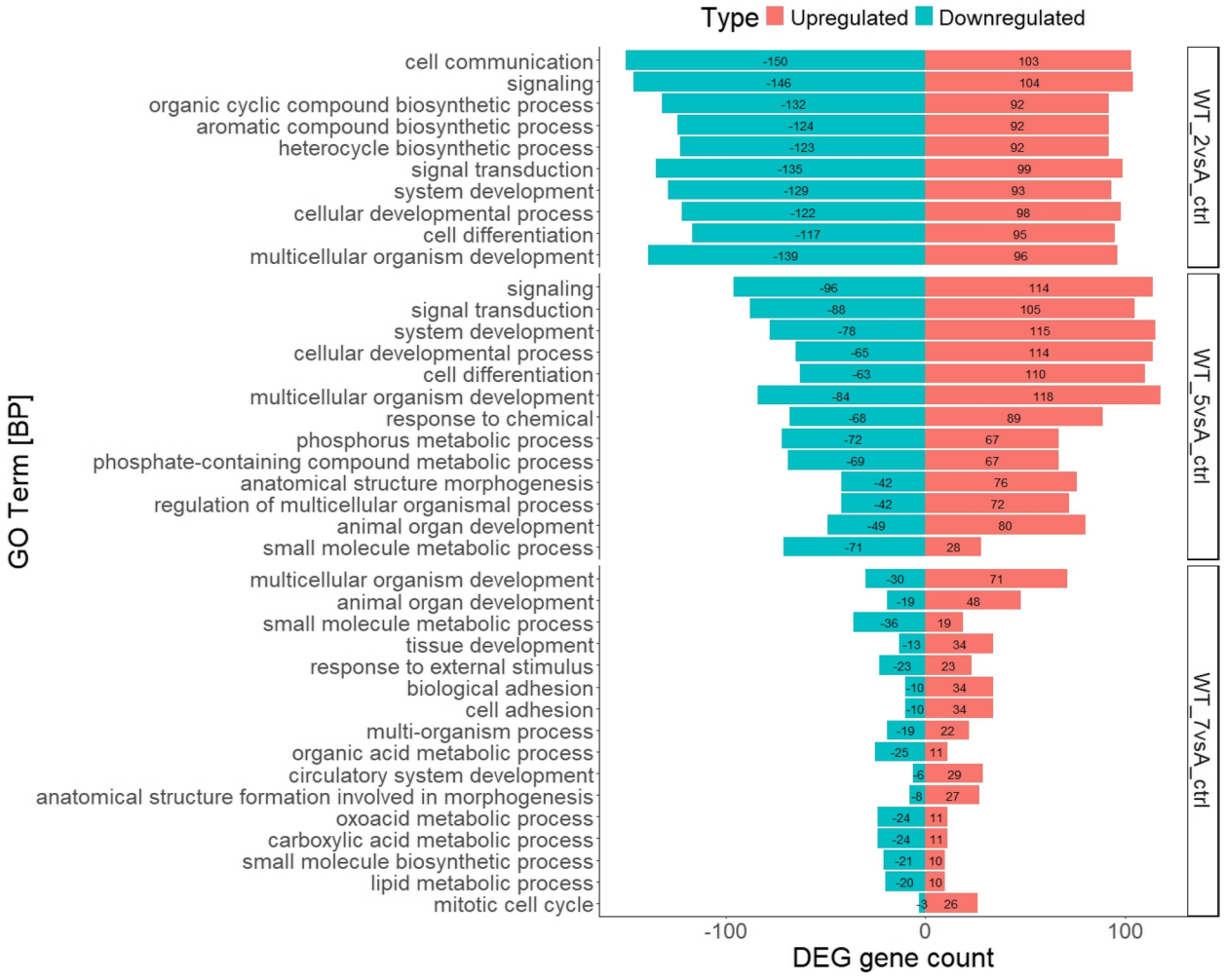

Fig. 7 Bar chart of Gene ontology term biological process (BP) classes with upregulated and downregulated Differentially expressed gene counts identified in WT_2vsA_ctrl, WT_5vsA_ctrl, and WT_7vsA_ctrl

UPMT1901-infected chickens provides critical insights into its pathogenesis. While no mortality or abnormal signs were observed in the control group, 16.67% mortality occurred in the infected group, with deaths at 4-dpi. Similarly, the gross liver lesions in infected chickens ranged from pale-yellow discoloration and swelling at early stages to severe friability and worsened texture by 7-dpi, suggesting progressive hepatic damage due to the infection (Fig. 2b, c, e, f). The firm, yellow discoloration in the liver of deceased chickens at 4-dpi potentially indicates the changing of color of liver as the first onset of severe IBH lesions, which the texture change intensified as the infection progressed. Despite the chance of survival, infected chickens beyond 5-dpi consistently displayed significant IBH-related gross lesions, which requires further studies to explain the potential of individual response towards FAdV-8b. Also, the histological analysis further corroborated these findings, revealing a strong correlation between gross lesions and microscopic abnormalities. Infected livers contained prominent INIBs at 4-dpi (Fig. 2iii), a hallmark of FAdV infection, reflecting active viral replication at the nuclei and cellular damage [4]. These findings were accompanied by disrupted hepatocyte architecture and porous sinusoids, with INIBs becoming less pronounced, but abnormal liver structures persisting at 7-dpi (Fig. 2vii). This clear association between gross lesions and the presence of INIBs highlights their role as key indicators of viral activity and damage. To confirm that the observed molecular and transcriptomic changes were directly associated with FAdV-8b infection, we quantified the viral genome copy numbers in liver tissues using qPCR. This assay provided molecular evidence of viral presence in the analysed samples, which is essential to establish a causal link between infection and host gene expression changes. In the infected group, high viral loads were detected as early as 2-dpi, peaked at 5-dpi, and declined by 7 dpi. In contrast, no viral genomes were detected in the uninfected

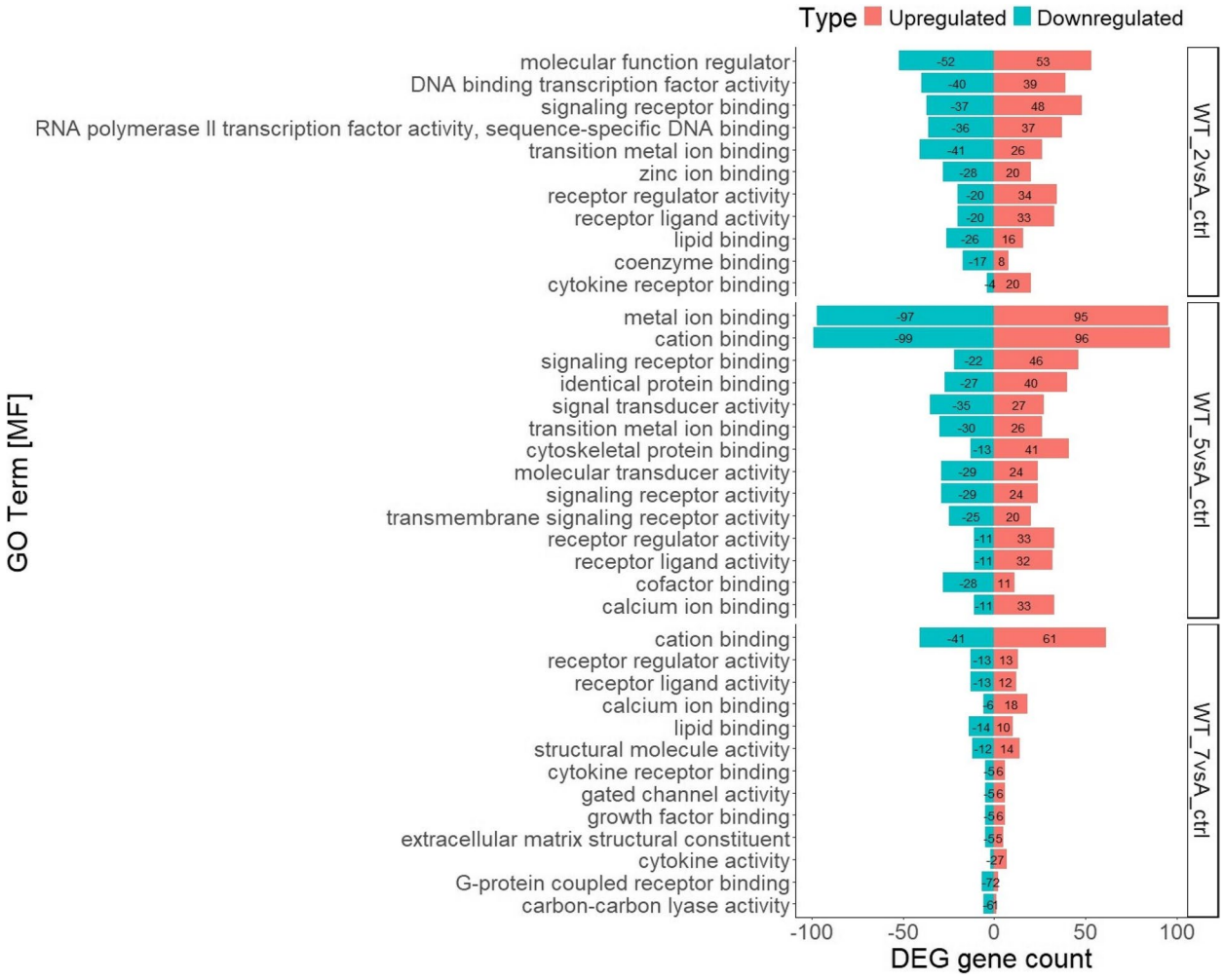

Fig. 8 Bar chart of Gene ontology term molecular function (MF) classes with upregulated and downregulated Differentially expressed gene counts identified in WT_2vsA_ctrl, WT_5vsA_ctrl, and WT_7vsA_ctrl

control group at any timepoint, validating the specificity of the assay and the infection status. These findings confirm the presence of FAdV-8b at the molecular level in the infected liver tissues, thereby justifying that the subsequent gene expression changes and alterations in signalling pathways observed via transcriptomic analysis are likely direct consequences of viral infection.

FAdV-8b infection has annotated to separate into three stages of incubation, degeneration, and convalescence up to 14-dpi, as proposed from the mortality, gross lesions, histology, and viral load reported [69]. Nevertheless, the pathogenesis of IBH disease is expected to remain up to 21-dpi, as several pathological and immunological studies have reported significant viral load and antibody detection in the wild-type FAdV-8b strain-infected birds, regardless of the genetics of chicken species [11, 19, 70, 71]. Upon inspection of the transcriptome profile, FAdV-8b infection can be categorized into virus incubation with genetic replication initiation, followed by the early and late stages of degeneration with major metabolite hijacking, proceeded with a high cell apoptosis. Interestingly, a higher number of DEGs reported from KEGG analysis is classified to enrich in immunity, viral replication, and cell cycle processes were only identified in WT_2 and WT_5, whereas WT_5 and WT_7 was primarily enriched in DEGs involved in metabolite hijacking. This suggested 5-dpi of FAdV-8b-infection to include all three major viral infections activities presence, uniquely in 2- and 7-dpi.

The viral entry of FAdV-8b intricates receptor binding functions and multiple signaling pathways, followed by membrane fusion and entry toward the cytoplasmic environment of liver cells. At the first stage of infection (0–2-dpi), we have detected significant down-regulation of the cell adhesion process, which potentially deregulated through viral hijacking to prevent cell–cell communication towards rapid immune response and allowing viral entry via endosomal activity [72–74]. Previously, this

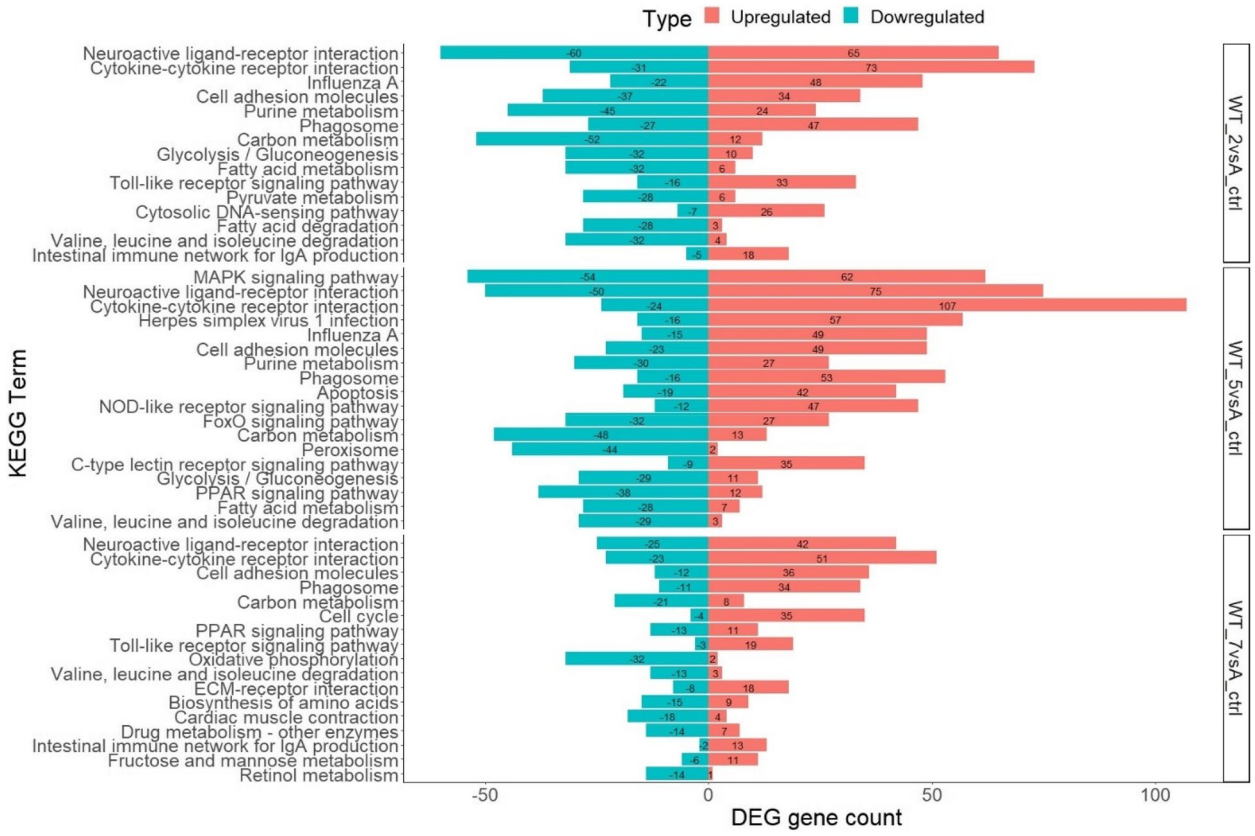

Fig. 9 Bar chart of KEGG term with upregulated and downregulated Differentially expressed genes counts identified in WT_2vsA_ctrl, WT_5vsA_ctrl, and WT_7vsA_ctrl

downregulation was also reported in both Human adenovirus [75] and FAdV-4 infection [15]. Interestingly, within the infected cells, immune-response-related genes are reported upregulated, whereas cell–cell adhesions genes are significantly downregulated. Next, genes involved in citrate cycle, glycolysis, and gluconeogenesis were reported to be significantly downregulated to ensure a successful abundance of viral entry into the cells, altering aerobic cellular respiration towards an anaerobic mechanism. This pattern is similarly recorded in amino acid profiling of FAdV-4-infected LMH cells, with the pathogen's ability to restore host's metabolism into TCA activation. The reduction in dependency on glucose for ATP production aligns with the Warburg effect which are seen in tumour formation and SARS-CoV-2 infection [76, 77], which alters the aerobic respiration towards lactate production and generates pools of nucleotide for viral replication within the aerobic environment [78, 79]. Similarly seen in the regulation of pyruvate metabolism, the up-regulation of LDH family, and down-regulation of ACAT enzyme, which involves the catabolism of fatty acids in mitochondria, ensuring the redirection of respiration in infected cells. Hence, subsequently, 2-dpi is reported with fatty acids degradation pathway to be significantly downregulated, with vital ACA and ACS families being downregulated and inhibiting the production of acetyl-CoA for bioenergy production in the citrate cycle, as well as viral envelope synthesis. Similarly, amino acids such as branched-chain amino acid (BCAA [valine, leucine, and isoleucine]), tryptophan, beta-alanine, alanine, aspartate, glutamate, and arginine, as well as carbon, retinol, and ester derivatives (propanoate and butanoate) metabolism pathways were downregulated. The synergy effect of reducing ester derivatives and accumulation of lysine promotes a blocking of viral infection, as seen in SARS-CoV-2 and Influenza A infection [80]. Adenovirus's ability to reduce the expression of NOS2 via arginine biosynthesis mechanism pathway has been elucidated to lead to a higher rate of replication and evading the host immune system [81], similar to the downregulations in 2-dpi of FAdV-8b-infected liver cells. Thus, arginine depletion in infected cells has been reported to reduce the viral replication rate of SARS-CoV-2 significantly, and it has been proposed as a therapeutic intervention [82–84]. The down-regulation of retinol metabolism in FAdV-8b-infected cells was also proposed as a viral-regulated decision as a previous study has hypothesized a fat-soluble retinol insufficiency may lead to an impaired immune system, risking significant inflammation against infection [85]. Due to the current rewiring of glycolysis

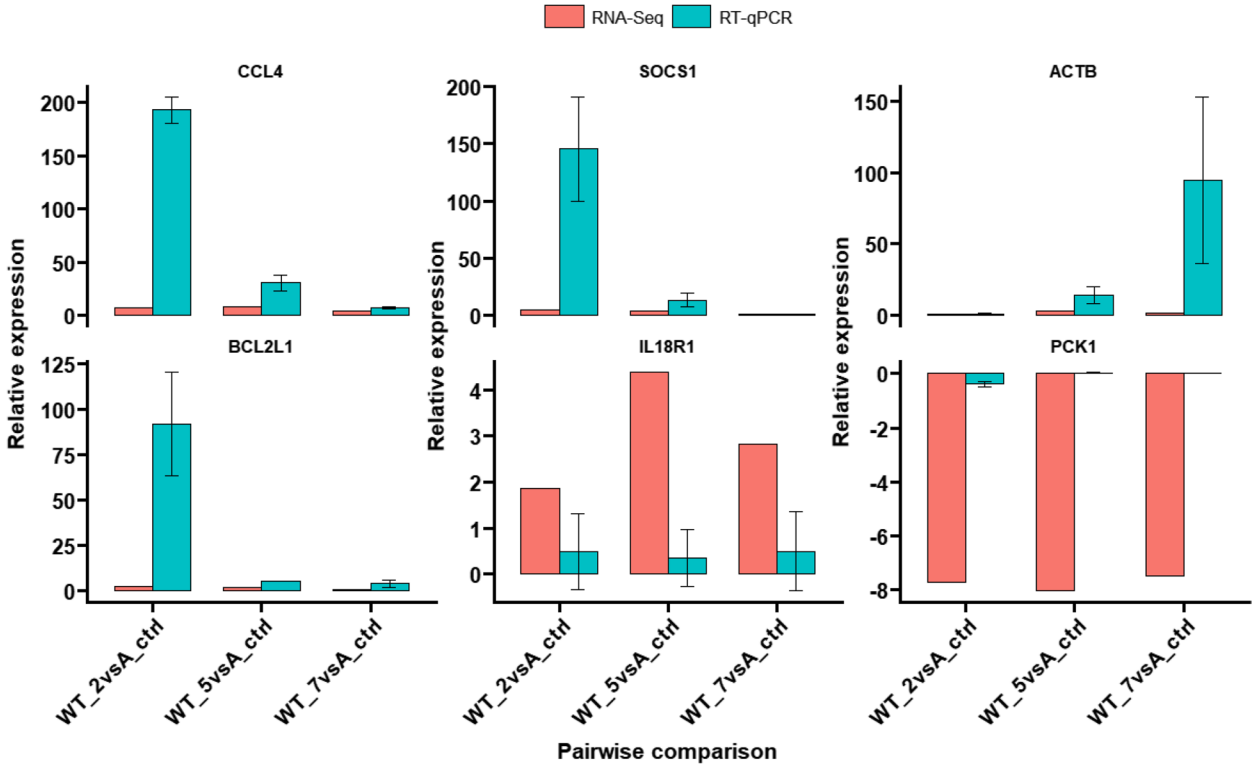

Fig. 10 Bar chart of expression levels comparison of six genes retrieved from RNA-Sequencing analysis and RT-qPCR, for validation purposes via the ΔΔCq calculation method. The retrieved in vitro RT-qPCR and in silico RNA-Seq analysis reported with $P > 0.05$ deeming non-statistically significant, ensuring the correlation between two results

and regular oxidative phosphorylation, the purine metabolism pathway is significantly downregulated, which elucidates an accumulation of nucleotides as the building block of viruses' unrestrained proliferations [86]. Nevertheless, down-regulation of the BCAA degradation pathway, which could lead to accumulation of BCAA, is proposed as an anti-viral response from the host as valine supplementation into viral hepatitis C virus (HCV)-patients were reported with ameliorated liver cirrhosis symptoms and HCV viral load [87]. The differentially expressed beta-alanine metabolism pathways in this stage of infection are due to viral hijacking, to create an optimum cellular environment for viral replication via carnosine [beta-alanine L-histidine] production, which was proven to inhibit dengue virus genome replication [88]. Despite the rewiring of metabolism processes at an early stage of infection, the host's innate immune responses, such as cytokine-cytokine receptor interaction, neuroactive ligand receptor interaction, Influenza A, phagosome, Toll-like receptor (TLR) signaling pathway, and intestinal immune network for IgA production pathways were significantly upregulated, triggering the innate immune response to fight against the entry of pathogens, as seen in FAdV-4 infections [15, 16]. Meanwhile, according to GO analysis, a set of genes expression utilizing RNA transcription and DNA replication molecular functions was only reported to be highly regulated in 2-dpi, suggesting transcription initiation at the ssDNA strand of FAdV-8b via the host's system at 2-dpi. These indicate 0- to 2-dpi as the most crucial time points for host–pathogen interaction, to mark the start of bioenergetics and biosynthetic demands of rapid viral replication by creating an optimum cellular environment and hidden from the host immune system via regulating the metabolite production and sudden onset of ATP, to prompt for the start of genomic replication.

Invaded viruses regulate the infected host's cell metabolism for replication, production, and release for their survival [89–91]. At 3–5-dpi, similar gene expression profiles enriched in the glycolysis and gluconeogenesis pathways are reported between 2- and 5-dpi, suggesting both of the pathways are a vital process for FAdV-8b infection in liver cells, a common mechanism of cell adaptation in various viral infections or viral-caused sepsis [78]. Furthermore, the ATP binding cassette (ABC) transporter pathway, one of the largest transport proteins superfamily abundance in the lipid-processing cells such as hepatocytes, is significantly downregulated, risking towards an abnormal lipid metabolism [92]. A declined expression of ABC transporter has been reported in the livers of humans infected with hepatitis C, a similar situation seen in chicken livers infected with FAdV-8b via manifestation

of INIB [93]. Correspondingly, the down-regulation of metabolomics pathways at this stage involves the metabolism of more metabolites such as nitrogen, a few additional amino acids (cysteine, methionine, glycine, serine, and threonine), and proline, also similarly seen in SARS-CoV-2 infection [94]. Meanwhile, the modulation of proline is hypothesized to prolong an infection of *Helicobacter pylori*, as proline flux is reported to coordinated the optimal growth of Gastric epithelial cells [95–97]. It was further reported that an abundance of serine antagonizes anti-viral innate immunity [98]. At the same time, glycine supplementation in human reduces possible flu infections by increasing the extracellular matrix as the mechanical barrier against infective agents [99], further elucidating FAdV-8b infected cell's modulation of the glycine, serine, and threonine metabolism pathway as a viral hijacking towards host immune response. Abundant list of metabolites have been reported to deregulate upon FAdV-8b infection significantly marks the start of the early degeneration stage, which elucidate the collapse of normal hepatocytes cellular activities, similar to the hypothesized disease of progression of FAdV-8b from lesion and histological reports. Interestingly, immune processes such as apoptosis, phagosome, Influenza A, Herpes simplex virus 1 infection, neuroactive ligand-receptor interaction, cytokine-cytokine receptor interaction, TLR, MAPK, and p53 signaling pathways, and more have significantly began to up-regulate, similarly seen in FAdV-4 infection of in vitro LMH [41]. During this stage, peroxisome and its subsequent PPAR signaling pathway processes were significantly downregulated, further supporting the notion of viral hijacking of metabolisms in preparation of a lipid-abundance environment (i.e. lipid homeostasis), potentially for virion encapsulation prior to release [100–103], survival, as well as modulating infections within host [101]. Additionally, the up-regulation STX12 [104] and F-actin genes [105, 106] enriched in the phagosome pathway identified at 5-dpi explicated the robust immune response in the infected cells via activation of autophagy and internalization into localized immune cells in the infected liver organ. Similar immune-related pathways have been identified in both 2- and 5-dpi, but with larger log2 fold change values at later stage, leading to further activation and regulation of the host's innate immune response to fight against the pathogens. However, the robust immune response promotes the FAdV-8b infected organ to be more prone to tissue damage, organ failure, or death, as seen in two deaths at 4-dpi death reported in this study. Meanwhile, the MAPK signaling pathway, p53 signaling pathway, NOD-like signaling pathway, and C-type lectin receptor (CLR) signaling pathway are uniquely reported at 5-dpi, interpreted as significantly upregulated except for FoxO signaling pathway reported as downregulated. The alteration of MAPK [107], CLR [108], and NOD-like signaling pathway [109] activates the transcription factor and control the inflammatory cytokines' expression, while p53 signaling pathway with the up-regulation of CASP family forces viral-infected cells into apoptosis [110, 111]. Meanwhile, the modulation of VISTA gene from cell adhesion molecules pathway and NFKBIA gene from adipocytokine signaling pathway, also proven to involve in regulation of T-cells activation in viral-infected cells [112, 113]. Accordingly, these upregulation of immune-related processes and down-regulation of cellular metabolism processes displayed a complex interplay situation between FAdV-8b and liver cells, for anti-viral defense or viral replication. The entry of FAdV-8b indeed induces strong and robust immune response at 3–5-dpi, while the host's liver cells enter a static phase of balanced offensive and defensive attacks, as well as major manipulation of the host cell metabolite machinery, in order to produce optimal progeny virion generation [114, 115].

At 6–7-dpi, lesser KEGG pathway processes are significantly regulated as compared to the previous stage of infection of 0- to 2-dpi and 3- to 5-dpi, leading FAdv-8b-infected liver tissue cells towards control and normal tissue gene-environment. However, more processes are differentially expressed from downregulated into upregulated, such as cell adhesion molecules, phagosomes, cytokine-cytokine receptor interaction, neuroactive ligand-receptor interaction, metabolism processes of galactose, fructose, mannose, alanine, aspartate, and glutamate. In contrast, the PPAR signaling pathways, amino acid biosynthesis, and cardiac muscle contractions are downregulated. These displayed the change of survival strategy from progeny generation into its spread via cell apoptosis. As compared to the previous stage of infection, 6–7-dpi has remained dependent on glycolysis for bioenergy as significant up-regulation of glycolytic enzymes has been reported [116–118]. Similarly, fructose, mannose, galactose and carbon metabolism pathways are still upregulated to provide ATP for cellular activities. The up-regulation of genes enriched in the cardiac muscle contraction pathway, act as critical regulators for ion-influx and efflux for ATP production emphasizing the increase of glucose uptake and glycolysis activity. The redirection from rapid aerobic glycolysis to oxidative phosphorylation halted the Warburg effect at 7-dpi. This projected a reduction in lactate production, marking a reduce rate of FAdV-8b virion encapsulation assembly. Next, genes involved in a V-type ATPase (ATP6V family) enriched in the oxidative phosphorylation pathway were seen upregulated, potentially involved in endosomal and lysosomal acidification, as well as autophagy [119], annotated as a crucial host cell infection step [120]. The endosomal acidification is reported to escape the endosomes post-viral entry by inducing vesicle budding and

collapsing in diphtheria toxin (DT) of *Escherichia coli*, leading to further pathogenesis in E.coli-infected site [121, 122]. It was expected that the significant up-regulation of the endosomal acidification to be identified at 7-dpi due to the robust viral entry, marking the start of virion release from 6–7-dpi, as well as the constant immune response from T-cells at the infected site. Hence, TLR signaling pathway with Myd88 gene, similarly seen to induced inflammatory response in FAdV-4 infected chickens [123], cytokine-cytokine receptor interaction pathway with CCL, IL, and CXCL families, as well as down-regulation of Prolactin family, indicating constant immune response at 7-dpi. Nevertheless, the significant regulation of F-actin to continue the phagosomes activation and internalization against pathogens, but without increment of maturation rate via STX12 in 5-dpi. This indicates that 6–7-dpi responded with on-going anti-viral defense, yet with lesser cytokine storm, preventing from major degeneration and ability to still elicit antibody via interferons and more. From these three stages of infections, it is determined that FAdV-8b infection is specific and targeted, via invading the host with regulation of expression to produce optimal environment for virion progeny generation. It is then followed by metabolite hijacking for virus survival by buying time and hiding from anti-viral response, then an imminent cell death for progeny release to adjacent cells, which eventually leads to gradual destruction of FAdV-8b infected cells. Virus regulate cell adhesion molecules via up-regulation to facilitate the viral release [124].

In this project, the time-interval decision for sampling in this study had effectively mimics the mortality pattern of FAdV-8b, allowing a dynamic view of gene expression changes over time, capturing the progression of the disease and immune response phases in infected chickens. Yet, the employment of the newly developed protocol of single-cell RNA-Sequencing (scRNA-Seq) will allow a more comprehensive overview of different cell populations within the liver of chicken, such as hepatocytes, Kupffer cells, stellate cells, and liver sinusoidal endothelial cells. Although the decision to pool the biological replicates into one pool omits the biological variations that could rise from different infected chickens, it is also recommended to investigate the potential individual variability after this study by sequencing biological replicates. Nevertheless, technical replicates performed during sequencing, strict pre-processing of raw reads, and holistic annotation against established databases such as GO and KEGG, facilitate the retrieval of our first transcriptomic profile of FAdV-8b infection, providing basis for future investigation of the infection.

Conclusion

The in silico transcriptomic study provided the first comprehensive, detailed and novel insights on the holistic IBH-positive liver tissue infected with FAdV-8b in a temporal manner. The age of SPF chickens carried out in this study mimics the young poultry age susceptible to FAdV-8b infection from the environment, ensuring the findings retrieved closely reflect the target host population, although without capturing the full timeline of the infection process, stopping at 7-dpi. Nevertheless, the findings mentioned upon the fate of the liver, accumulation of activated immune cells post-triggering of immune response up to 7-dpi, as well as the rewiring of the environment for viral survival have elucidated a major interplay that fully depends on the strength and prowess of both the pathogen and the host such as metabolite hijacking which peaked at 5-dpi. The data obtained through this study proposed the mechanisms behind the FAdV-8b invasion in a series of timelines, from early viral invasion towards the establishment of the adaptive immune response state. The abnormal lipid metabolism observed in gross lesions, histological findings, and regulated fatty acid metabolism pathways in FAdV-8b infected liver tissues may play a significant role in pathogen infection, influencing both viral propagation and immune evasion. Overall, the data obtained elucidate the complexity of FAdV-8b and host interactions, which can be utilized as the building blocks for novel putative molecular targets for prognostic assessment, or as an ameliorative intervention for vaccine production or amino acid therapy.

Fundings

This work was mainly funded by the Higher Institute Centre of Excellence (HICoE) [grant number 5220002] from the Ministry of Higher Education (MOHE) of the Malaysian government and supported by the Geran Putra-Inisiatif Putra Siswazah (GP-IPS) [grant number 9705400] from Universiti Putra Malaysia.

Supplementary Information

The online version contains supplementary material available at https://doi.org/10.1186/s12864-025-11853-x.

Supplementary Material 1.

Acknowledgements

Not applicable.

Authors' contributions

B.A. determined the experimental design, performed the trial experiments, analysed the data, performed the statistical data, and drafted the final manuscript. N.F.S. and C.C.U. also assisted throughout animal trial experiment. N.M.I. co-conceived the study by participating in the design of the molecular work stages of the project. M.H.B. and N.M.S. provided insights, guidance on planning, and assistance during animal design and trial. N.A.W.A.H. provided guidance and technical servers to perform bioinformatics analysis of the transcriptomics library. N.M.I. guided during experimental design,

interpretation of the results and conclusion. All authors contributed to the manuscript's text and content, including the revisions and edits. All authors approve the content of the final manuscript and agree to be held accountable for the work done.

Data availability

The datasets of raw reads sequences used in supporting this study's article are available in the National Center of Biotechnology Information (NCBI) BioProject no. PRJNA1059483, [https://www.ncbi.nlm.nih.gov/bioproject/PRJNA1059483].

Declarations

Ethics approval and consent to participate

The animal trial experiment carried out in this study was conducted with the approval of the International Animal Care and Use Committee [No: UPM/IACUC/AUP-R065/2020].

Consent for publication

Not applicable.

Competing interests

The authors declare no competing interests.

Received: 5 August 2024 / Accepted: 24 June 2025
Published online: 25 July 2025

References

1. Benkö M, Harrach B, Both GW, Russell WC, Adair BM, Ádám É, et al. Family Adenoviridae Virus Taxanomy. 2005;8:213–28.
2. Niczyporuk JS, Woźniakowski G, Samorek-Salamonowicz E. Application of cross-priming amplification (CPA) for detection of fowl adenovirus (FAdV) strains. Arch Virol. 2015;160(4):1005–13. Available from: http://link.springer.com/10.1007/s00705-015-2355-9.
3. Steer PA, Kirkpatrick NC, O'Rourke D, Noormohammadi AH. Classification of fowl adenovirus serotypes by use of high-resolution melting-curve analysis of the hexon gene region. J Clin Microbiol. 2009;47(2):311–21. Available from: https://jcm.asm.org/content/47/2/311.
4. El-Shall NA, El-Hamid HSA, Elkady MF, Ellakany HF, Elbestawy AR, Gado AR, et al. Epidemiology, pathology, prevention, and control strategies of inclusion body hepatitis and hepatitis-hydropericardium syndrome in poultry: A comprehensive review. Front Vet Sci. 2022;9. Available from:https://www.frontiersin.org/articles/10.3389/fvets.2022.963199/full.
5. Mo K kun, Lyu C fei, Cao S shang, Li X, Xing G, Yan Y, et al. Pathogenicity of an FAdV-4 isolate to chickens and its genomic analysis. J Zhejiang Univ B. 2019;20(9):740–52. Available from: http://link.springer.com/10.1631/jzus.B1900070.
6. Wang Z, Zhao J. Pathogenesis of Hypervirulent Fowl Adenovirus Serotype 4: The Contributions of Viral and Host Factors. Viruses. 2019;11(8):741. Available from: https://www.mdpi.com/1999-4915/11/8/741.
7. Jakab S, Bali K, Homonnay Z, Kaszab E, Ihász K, Fehér E, et al. Genomic Epidemiology and Evolution of Fowl Adenovirus 1. Animals. 2023;13(18):2819. Available from: https://www.mdpi.com/1999-4915/11/8/741.
8. Chen H, Li M, Liu S, Kong J, Li D, Feng J, et al. Whole-genome sequence and pathogenicity of a fowl adenovirus 5 isolated from ducks with egg drop syndrome in China. Front Vet Sci. 2022;9:961793. Available from: http://www.ncbi.nlm.nih.gov/pubmed/36032289.
9. Marek A, Kaján GL, Kosiol C, Benkő M, Schachner A, Hess M. Genetic diversity of species Fowl aviadenovirus D and Fowl aviadenovirus E. J Gen Virol. 2016;97(9):2323–32. Available from: https://www.microbiologyresearch.org/content/journal/jgv/10.1099/jgv.0.000519.
10. Norina L, Norsharina A, Nurnadiah AH, Redzuan I, Ardy A, Nor-Ismaliza I. Avian Adenovirus Isolated From Broiler Affected With Inclusion Body Hepatitis. Avian Adenovirus Isol From Broiler Affect With Incl Body Hepat. 2016;Volume 7:121–6. Available from: http://www.dvs.gov.my/dvs/resources/user_14/MJVR_V7N2/MJVR-V7N2-p121-126.pdf.
11. Sohaimi NM, Clifford UC. Fowl adenovirus in chickens: Diseases, epidemiology, impact, and control strategies to the Malaysian poultry industry- a review. J World's Poult Res. 2021;11(3):387–96. Available from: https://jwpr.science-line.com/attachments/article/59/JWPR 11(3) 387–396, 2021.pdf
12. Sohaimi NM, Hair-Bejo M. A recent perspective on fiber and hexon genes proteins analyses of fowl adenovirus towards virus infectivity - A review. Open Vet J. 2021;11(4):569. Available from: https://www.ejmanager.com/fulltextpdf.php?mno=98642.
13. Majdi A, Hair-Bejo M. Pathogenecity of Malaysian fowl adenovirus isolates in specific pathogen free chickens. In: 10th Proceeding of the Seminar of Veterinary Sciences. Faculty of Veterinary Medicine, Universiti Putra Malaysia; 2015. p. 15–20.
14. Sohaimi NM, Omar AR, Ideris A. Molecular detection and pathogenicity of fowl adenovirus. Int J Agric Sci Vet Med. 2018;6(1).
15. Wang XP, Wen B, Zhang XJ, Ma L, Liang XL, Zhang ML. Transcriptome Analysis of Genes Responding to Infection of Leghorn Male Hepatocellular Cells With Fowl Adenovirus Serotype 4. Front Vet Sci. 2022;9. Available from: https://www.frontiersin.org/articles/10.3389/fvets.2022.871038/full.
16. Ren G, Wang H, Huang M, Yan Y, Liu F, Chen R. Transcriptome analysis of fowl adenovirus serotype 4 infection in chickens. Virus Genes. 2019;55(5):619–29. Available from: http://link.springer.com/10.1007/s11262-019-01676-w.
17. Pilkington P, Brown T, Villegas P, McMurray B, Page RK, Rowland GN, et al. Adenovirus-induced inclusion body hepatitis in four-day-old broiler breeders. Avian Dis. 1997;41(2):472–4. Available from: http://www.ncbi.nlm.nih.gov/pubmed/9201418.
18. Hair-Bejo M. Inclusion body hepatitis in a flock of a commercial broilers chickens. J Vet Malaysia. 2005;31:23–6.
19. Mat Isa N, Mohd Ayob J, Ravi S, Mustapha NA, Ashari KS, Bejo MH, et al. Complete genome sequence of fowl adenovirus-8b UPM04217 isolate associated with the inclusion body hepatitis disease in commercial broiler chickens in Malaysia reveals intermediate evolution. VirusDisease. 2019;30(3):426–32. Available from: http://link.springer.com/10.1007/s13337-019-00530-9.
20. Sohaimi NM, Hair-Bejo M, Omar AR, Ideris A, Isa NM. Hexon and fiber gene changes in an attenuated fowl adenovirus isolate from Malaysia in embryonated chicken eggs and its infectivity in chickens. J Vet Sci. 2018;19(6):759–70.
21. Ahmed S, Mariatulqabtiah AR, Bejo MH, Omar AR, Ideris A, Mat Isa N. Molecular markers and phylogenetic analysis of UPMT27, a field isolate of the Malaysian fowl adenovirus associated with inclusion body hepatitis. Pertanika J Sci Technol. 2021;29(1). Available from: http://www.pertanika.upm.edu.my/pjst/browse/regular-issue?article=JST-2013-2020.
22. Azli B, Salim NF, Omar AR, Hair-Bejo M, Sohaimi NM, Isa NM. Molecular Characterisation of Partial Structural Genes of Fowl Adenovirus Serotype 8b UPMT1901 Field Strain Isolate Associated with the Inclusion Body Hepatitis in Malaysia's Commercial Broiler Chickens. Pertanika J Trop Agric Sci. 2023;46(3):1003–26.
23. Sabarudin NS, Tan SW, Phang YF, Omar AR. Molecular characterization of Malaysian fowl adenovirus (FAdV) serotype 8b species E and pathogenicity of the virus in specific-pathogen-free chicken. J Vet Sci. 2021;22(4). Available from: https://vetsci.org/x.php?id=10.4142/jvs.2021.22.e42.
24. Schachner A, Gonzalez G, Endler L, Ito K, Hess M. Fowl Adenovirus (FAdV) Recombination with Intertypic Crossovers in Genomes of FAdV-D and FAdV-E, Displaying Hybrid Serological Phenotypes. Viruses. 2019;11(12):1094. Available from: https://www.mdpi.com/1999-4915/11/12/1094.
25. Schachner A, Grafl B, Hess M. Spotlight on avian pathology: Fowl adenovirus (FAdV) in chickens and beyond– an unresolved host-pathogen interplay. Avian Pathol. 2021 Jan 2;50(1):2–5. Available from: https://www.tandfonline.com/doi/full/10.1080/03079457.2020.1810629.
26. Hess M. Detection and differentiation of avian adenoviruses: A review. Avian Pathol. 2000;29(3):195–206. Available from: http://www.tandfonline.com/doi/full/10.1080/03079450050045440.
27. Steer PA, Sandy JR, O'Rourke D, Scott PC, Browning GF, Noormohammadi AH. Chronological analysis of gross and histological lesions induced by field strains of fowl adenovirus serotypes 1, 8b and 11 in one-day-old chickens. Avian Pathol. 2015;44(2):106–13. Available from: http://www.tandfonline.com/doi/abs/10.1080/03079457.2015.1007919.
28. Niu Y juan, Sun W, Zhang G hua, Qu Y jin, Wang P fei, Sun H lei, et al. Hydropericardium syndrome outbreak caused by fowl adenovirus serotype 4 in China in 2015. J Gen Virol. 2016;97(10):2684–90. Available from: https://www.microbiologyresearch.org/content/journal/jgv/10.1099/jgv.0.000567.
29. Quigley M, Martinez J, Huang X, Yang Y. A critical role for direct TLR2-MyD88 signaling in CD8 T-cell clonal expansion and memory formation following vaccinia viral infection. Blood. 2009;113(10):2256–64. Available from: https://ashpublications.org/blood/article/113/10/2256/24336/A-critical-role-for-direct-TLR2MyD88-signaling-in.

30. Li C, Wang T, Zhang Y, Wei F. Evasion mechanisms of the type I interferons responses by influenza A virus. Crit Rev Microbiol. 2020;46(4):420–32. Available from: https://www.tandfonline.com/doi/full/10.1080/1040841X.2020.1794791.
31. Yu J, Sun X, Goie JYG, Zhang Y. Regulation of Host Immune Responses against Influenza A Virus Infection by Mitogen-Activated Protein Kinases (MAPKs). Microorganisms. 2020;8(7):1067. Available from: https://www.mdpi.com/2076-2607/8/7/1067.
32. Toscano MG, de Haan P. How Simian Virus 40 Hijacks the Intracellular Protein Trafficking Pathway to Its Own Benefit… and Ours. Front Immunol. 2018;9. Available from:https://www.frontiersin.org/article/10.3389/fimmu.2018.01160/full.
33. Wang Q, Wang Z, Zhang J, Zhang Q, Zheng M, Wen J, et al. Dual RNA-Seq of H5N1 Avian Influenza Virus and Host Cell Transcriptomes Reveals Novel Insights Into Host-Pathogen Cross Talk. Front Microbiol. 2022;13. Available from: https://www.frontiersin.org/articles/10.3389/fmicb.2022.828277/full.
34. De Conto F. Avian Influenza A Viruses Modulate the Cellular Cytoskeleton during Infection of Mammalian Hosts. Pathogens. 2024;13(3):249. Available from: https://www.mdpi.com/2076-0817/13/3/249.
35. Liang Y. Pathogenicity and virulence of influenza. Virulence. 2023 Dec;14(1):2223057. Available from: http://www.ncbi.nlm.nih.gov/pubmed/37339323.
36. Connolly PF, Fearnhead HO. Viral hijacking of host caspases: an emerging category of pathogen–host interactions. Cell Death Differ. 2017;24(8):1401–10. Available from: https://www.nature.com/articles/cdd201759.
37. Sen R, Nayak L, De RK. A review on host–pathogen interactions: classification and prediction. Eur J Clin Microbiol Infect Dis. 2016;35(10):1581–99. Available from: http://link.springer.com/10.1007/s10096-016-2716-7.
38. Mundade R, Ozer HG, Wei H, Prabhu L, Lu T. Role of ChIP-seq in the discovery of transcription factor binding sites, differential gene regulation mechanism, epigenetic marks and beyond. Cell Cycle. 2014;13(18):2847–52. Available from: http://www.tandfonline.com/doi/full/10.4161/15384101.2014.949201.
39. Dorado G, Gálvez S, Rosales TE, Vásquez VF, Hernández P. Analyzing Modern Biomolecules: The Revolution of Nucleic-Acid Sequencing - Review. Biomolecules. 2021;11(8). Available from: http://www.ncbi.nlm.nih.gov/pubmed/34439777.
40. Ahmed W. RNA-seq resolving host-pathogen interactions: Advances and applications. Ecol Genet Genomics. 2020;15:100057. Available from: https://linkinghub.elsevier.com/retrieve/pii/S2405985420300069.
41. Wu N, Yang B, Wen B, Wang T, Guo J, Qi X, et al. Interactions Among Expressed MicroRNAs and mRNAs in the Early Stages of Fowl Adenovirus Aerotype 4-Infected Leghorn Male Hepatocellular Cells. Front Microbiol. 2020;11(May):1–18.
42. Liu XN, Guo XR, Han Y, Tian T, Sun J, Lei BS, et al. The Cellular and Viral circRNAs Induced by Fowl Adenovirus Serotype 4 Infection. Front Microbiol. 2022;13:925953. Available from: http://www.ncbi.nlm.nih.gov/pubmed/35722302.
43. Ji WT, Liu H. PI3K-Akt Signaling and Viral Infection. Recent Pat Biotechnol. 2008;2(3):218–26. Available from: http://www.eurekaselect.com/openurl/content.php?genre=article&issn=1872-2083&volume=2&issue=3&spage=218.
44. Diehl N, Schaal H. Make Yourself at Home: Viral Hijacking of the PI3K/Akt Signaling Pathway. Viruses. 2013 Dec 16;5(12):3192–212. Available from: https://www.mdpi.com/1999-4915/5/12/3192.
45. Carty M, Bowie AG. Recent insights into the role of Toll-like receptors in viral infection. Clin Exp Immunol. 2010;161(3):397–406. Available from: https://academic.oup.com/cei/article/161/3/397/6438672.
46. Duan T, Du Y, Xing C, Wang HY, Wang RF. Toll-Like Receptor Signaling and Its Role in Cell-Mediated Immunity. Front Immunol. 2022;13. Available from: https://www.frontiersin.org/articles/10.3389/fimmu.2022.812774/full.
47. Zhang Y, Li BX, Mao QZ, Zhuo JC, Huang HJ, Lu JB, et al. The JAK-STAT pathway promotes persistent viral infection by activating apoptosis in insect vectors. Tao X, editor. PLOS Pathog. 2023;19(3):e1011266. Available from: https://dx.plos.org/10.1371/journal.ppat.1011266.
48. Xiang S, Huang R, He Q, Xu L, Wang C, Wang Q. Arginine regulates inflammation response-induced by Fowl Adenovirus serotype 4 via JAK2/STAT3 pathway. BMC Vet Res. 2022;18(1):189. Available from: https://bmcvetres.biomedcentral.com/articles/10.1186/s12917-022-03282-9.
49. Chen Y, Huang R, Qu G, Peng Y, Xu L, Wang C, et al. Transcriptome Analysis Reveals New Insight of Fowl Adenovirus Serotype 4 Infection. Front Microbiol. 2020;11. Available from: https://www.frontiersin.org/article/10.3389/fmicb.2020.00146/full.
50. Suvarna SK, Bancroft JD, Layton C. Bancroft's Theory and Practice of Histological Techniques. Elsevier; 2019. Available from: https://linkinghub.elsevier.com/retrieve/pii/C20150001435.
51. McIntyre LM, Lopiano KK, Morse AM, Amin V, Oberg AL, Young LJ, et al. RNA-seq: technical variability and sampling. BMC Genomics. 2011;12(1):293. Available from: https://bmcgenomics.biomedcentral.com/articles/10.1186/1471-2164-12-293.
52. Andrew S. FASTQC. A quality control tool for high throughput sequence data. 2010;
53. jstjohn. SeqPrep: Tool for stripping adaptors and/or merging paired reads with overlap into single reads.. 2016. Available from: https://github.com/jstjohn/SeqPrep. [cited 2021 Sep 5].
54. Joshi N, Fass J. Sickle: A sliding-window, adaptive, quality-based trimming tool for FastQ files [Software]. 2011. Available from: https://github.com/najoshi/sickle.
55. International Chicken Genome Sequencing Consortium. Sequence and comparative analysis of the chicken genome provide unique perspectives on vertebrate evolution. Nature. 2004;432(7018):695–716. Available from: https://www.nature.com/articles/nature03154.
56. Kim D, Paggi JM, Park C, Bennett C, Salzberg SL. Graph-based genome alignment and genotyping with HISAT2 and HISAT-genotype. Nat Biotechnol. 2019;37(8):907–15. Available from: https://www.nature.com/articles/s41587-019-0201-4.
57. Pertea M, Pertea GM, Antonescu CM, Chang TC, Mendell JT, Salzberg SL. StringTie enables improved reconstruction of a transcriptome from RNA-seq reads. Nat Biotechnol. 2015;33(3):290–5. Available from: http://www.ncbi.nlm.nih.gov/pubmed/25690850.
58. Liao Y, Smyth GK, Shi W. featureCounts: an efficient general purpose program for assigning sequence reads to genomic features. Bioinformatics. 2014;30(7):923–30. Available from: https://academic.oup.com/bioinformatics/article/30/7/923/232889.
59. Robinson MD, McCarthy DJ, Smyth GK. edgeR: a Bioconductor package for differential expression analysis of digital gene expression data. Bioinformatics. 2010;26(1):139–40. Available from: https://academic.oup.com/bioinformatics/article/26/1/139/182458.
60. Ashburner M, Ball CA, Blake JA, Botstein D, Butler H, Cherry JM, et al. Gene ontology: tool for the unification of biology. The Gene Ontology Consortium. Nat Genet. 2000;25(1):25–9. Available from: http://www.ncbi.nlm.nih.gov/pubmed/10802651.
61. Kanehisa M. KEGG: Kyoto Encyclopedia of Genes and Genomes. Nucleic Acids Res. 2000;28(1):27–30. Available from: https://academic.oup.com/nar/article-lookup/doi/10.1093/nar/28.1.27.
62. Yu G, Wang LG, Han Y, He QY. clusterProfiler: an R package for comparing biological themes among gene clusters. OMICS. 2012;16(5):284–7. Available from: http://www.ncbi.nlm.nih.gov/pubmed/22455463.
63. Wickham H. ggplot2: Elegant Graphics for Data Analysis. Springer-Verlag New York; 2016. Available from: https://ggplot2.tidyverse.org.
64. Subramanian A, Tamayo P, Mootha VK, Mukherjee S, Ebert BL, Gillette MA, et al. Gene set enrichment analysis: A knowledge-based approach for interpreting genome-wide expression profiles. Proc Natl Acad Sci. 2005;102(43):15545–50. Available from: https://pnas.org/doi/full/10.1073/pnas.0506580102.
65. Mackay IM. Real-time PCR in virology. Nucleic Acids Res. 2002;30(6):1292–305. Available from: https://academic.oup.com/nar/article-lookup/doi/10.1093/nar/30.6.1292.
66. Livak KJ, Schmittgen TD. Analysis of Relative Gene Expression Data Using Real-Time Quantitative PCR and the 2−ΔΔCT Method. Methods. 2001;25(4):402–8. Available from: https://linkinghub.elsevier.com/retrieve/pii/S1046202301912629.
67. IBM. IBM SPSS Statistics for Windows. 2019.
68. McCarthy DJ, Chen Y, Smyth GK. Differential expression analysis of multifactor RNA-Seq experiments with respect to biological variation. Nucleic Acids Res. 2012;40(10):4288–97. Available from: https://academic.oup.com/nar/article/40/10/4288/2411520.
69. Steer-Cope P, Sandy J, O'Rourke D, Scott P, Browning G, Noormohammadi A. Chronologic Analysis of Gross and Histologic Lesions Induced by Field Strains of FAdV-1, FAdV-8b, and FAdV-11 in Six-Week-Old Chickens. Avian Dis. 2017;61(4):512. Available from: https://bioone.org/journals/avian-diseases/volume-61/issue-4/11718–072317-Reg.1/Chronologic-Analysis-of-Gross-and-Histologic-Lesions-Induced-by-Field/10.1637/11718-072317-Reg.1.full.

70. Ahmed S. Development of a live attenuated vaccine against fowl adenovirus by mutating fiber gene using CRISPR-Cas9 technology. University Putra Malaysia; 2021.
71. Zhang X, Liu L, Wang F, Li H, Fan J, Xie J, et al. Pathogenicity and innate immune responses induced by fowl adenovirus serotype 8b in specific pathogen-free chicken. Poult Sci. 2023;102(8):102846. Available from: https://linkinghub.elsevier.com/retrieve/pii/S0032579123003656.
72. Bhella D. The role of cellular adhesion molecules in virus attachment and entry. Philos Trans R Soc B Biol Sci. 2015;370(1661):20140035. Available from: https://royalsocietypublishing.org/doi/10.1098/rstb.2014.0035.
73. Mateo M, Generous A, Sinn PL, Cattaneo R. Connections matter – how viruses use cell–cell adhesion components. J Cell Sci. 2015;128(3):431–9. Available from: https://journals.biologists.com/jcs/article/128/3/431/55353/Connections-matter-how-viruses-use-cell-cell.
74. Harjunpää H, Llort Asens M, Guenther C, Fagerholm SC. Cell Adhesion Molecules and Their Roles and Regulation in the Immune and Tumor Microenvironment. Front Immunol. 2019 May 22;10. Available from: https://www.frontiersin.org/article/https://doi.org/10.3389/fimmu.2019.01078/full.
75. Rajala MS, Rajala RVS, Astley RA, Butt AL, Chodosh J. Corneal Cell Survival in Adenovirus Type 19 Infection Requires Phosphoinositide 3-Kinase/Akt Activation. J Virol. 2005;79(19):12332–41. Available from: https://journals.asm.org/doi/10.1128/JVI.79.19.12332-12341.2005.
76. Pouysségur J, Marchiq I, Parks SK, Durivault J, Ždralević M, Vucetic M. 'Warburg effect' controls tumor growth, bacterial, viral infections and immunity–Genetic deconstruction and therapeutic perspectives. Semin Cancer Biol. 2022;86:334–46. Available from: https://linkinghub.elsevier.com/retrieve/pii/S1044579X22001754.
77. Icard P, Lincet H, Wu Z, Coquerel A, Forgez P, Alifano M, et al. The key role of Warburg effect in SARS-CoV-2 replication and associated inflammatory response. Biochimie. 2021;180:169–77. Available from: http://www.ncbi.nlm.nih.gov/pubmed/33189832.
78. Zhang P, Pan S, Yuan S, Shang Y, Shu H. Abnormal glucose metabolism in virus associated sepsis. Front Cell Infect Microbiol. 2023;13. Available from: https://www.frontiersin.org/articles/10.3389/fcimb.2023.1120769/full.
79. Sanchez EL, Lagunoff M. Viral activation of cellular metabolism. Virology. 2015;479–480:609–18. Available from: https://linkinghub.elsevier.com/retrieve/pii/S0042682215000847.
80. Melano I, Kuo LL, Lo YC, Sung PW, Tien N, Su WC. Effects of Basic Amino Acids and Their Derivatives on SARS-CoV-2 and Influenza-A Virus Infection. Viruses. 2021;13(7):1301. Available from: https://www.mdpi.com/1999-4915/13/7/1301.
81. Luiking YC, Poeze M, Ramsay G, Deutz NEP. The Role of Arginine in Infection and Sepsis. J Parenter Enter Nutr. 2005;29(1S). Available from: https://aspenjournals.onlinelibrary.wiley.com/doi/10.1177/0148607105029051S70.
82. Raška K, Prage L, Schlesinger RW. Effects of arginine starvation on macromolecular synthesis in infection with type 2 adenovirus. Virology. 1972;48(2):472–84. Available from: https://linkinghub.elsevier.com/retrieve/pii/004268227290058X.
83. Xiang S, Huang R, He Q, Xu L, Wang C, Wang Q. Arginine regulates inflammation response-induced by Fowl Adenovirus serotype 4 via JAK2/STAT3 pathway. BMC Vet Res. 2022;18(1):1–10. Available from: https://doi.org/10.1186/s12917-022-03282-9.
84. Grimes JM, Khan S, Badeaux M, Rao RM, Rowlinson SW, Carvajal RD. Arginine depletion as a therapeutic approach for patients with COVID-19. Int J Infect Dis. 2021;102:566–70. Available from: https://linkinghub.elsevier.com/retrieve/pii/S1201971220323043.
85. Behboudi E, Zeynali P, Zahedian Nezhad N, Hamidi Sofiani V. Vitamin A and Viral Infection in Critical Care. Jorjani Biomed J. 2022;10(1):67–83. Available from: http://goums.ac.ir/jorjanijournal/article-1-876-en.html.
86. Ariav Y, Ch'ng JH, Christofk HR, Ron-Harel N, Erez A. Targeting nucleotide metabolism as the nexus of viral infections, cancer, and the immune response. Sci Adv. 2021;7(21). Available from: https://www.science.org/doi/10.1126/sciadv.abg6165.
87. Kawaguchi T, Torimura T, Takata A, Satomi S, Sata M. Valine, a Branched-Chain Amino Acid, Reduced HCV Viral Load and Led to Eradication of HCV by Interferon Therapy in a Decompensated Cirrhotic Patient. Case Rep Gastroenterol. 2012;6(3):660–7. Available from: https://karger.com/CRG/article/doi/10.1159/000343094.
88. Rothan HA, Abdulrahman AY, Khazali AS, Nor Rashid N, Chong TT, Yusof R. Carnosine exhibits significant antiviral activity against Dengue and Zika virus. J Pept Sci. 2019;25(8). Available from: https://onlinelibrary.wiley.com/doi/10.1002/psc.3196.
89. Thaker SK, Ch'ng J, Christofk HR. Viral hijacking of cellular metabolism. BMC Biol. 2019;17(1):59. Available from: https://bmcbiol.biomedcentral.com/articles/10.1186/s12915-019-0678-9.
90. Harries PA, Schoelz JE, Nelson RS. Intracellular Transport of Viruses and Their Components: Utilizing the Cytoskeleton and Membrane Highways. Mol Plant-Microbe Interact. 2010;23(11):1381–93. Available from: https://apsjournals.apsnet.org/doi/10.1094/MPMI-05-10-0121.
91. Mesquita I, Estaquier J. Viral Manipulation of the Host Metabolic Network. In 2018. p. 377–401. Available from: http://link.springer.com/10.1007/978-3-319-74932-7_10.
92. Ye Z, Lu Y, Wu T. The impact of ATP-binding cassette transporters on metabolic diseases. Nutr Metab (Lond). 2020;17(1):61. Available from: https://nutritionandmetabolism.biomedcentral.com/articles/10.1186/s12986-020-00478-4.
93. Hinoshita E, Taguchi K ichi, Inokuchi A, Uchiumi T, Kinukawa N, Shimada M, et al. Decreased expression of an ATP-binding cassette transporter, MRP2, in human livers with hepatitis C virus infection. J Hepatol. 2001;35(6):765–73. Available from: https://linkinghub.elsevier.com/retrieve/pii/S0168827801002161.
94. Federica G, Giuseppina F, Veronica L, Gianpaolo Z, Massimo T, Veronica DM, et al. An untargeted metabolomic approach to investigate antiviral defence mechanisms in memory leukocytes secreting anti-SARS-CoV-2 IgG in vitro. Sci Rep. 2023;13(1):629. Available from: https://www.nature.com/articles/s41598-022-26156-4.
95. Tanner JJ. Structural biology of proline catabolism. Amino Acids. 2008;35(4):719–30. Available from: http://link.springer.com/10.1007/s00726-008-0062-5.
96. Van Amsterdam K, Van Der Ende A. Nutrients Released by Gastric Epithelial Cells Enhance Helicobacter pylori Growth. Helicobacter. 2004;9(6):614–21. Available from: https://onlinelibrary.wiley.com/doi/10.1111/j.1083-4389.2004.00272.x.
97. Christgen SL, Becker DF. Role of Proline in Pathogen and Host Interactions. Antioxid Redox Signal. 2019;30(4):683–709. Available from: https://www.liebertpub.com/doi/10.1089/ars.2017.7335.
98. Shen L, Hu P, Zhang Y, Ji Z, Shan X, Ni L, et al. Serine metabolism antagonizes antiviral innate immunity by preventing ATP6V0d2-mediated YAP lysosomal degradation. Cell Metab. 2021;33(5):971–987.e6. Available from: https://linkinghub.elsevier.com/retrieve/pii/S1550413121001133.
99. Meléndez-Hevia E, de Paz-Lugo P, Sánchez G. Glycine can prevent and fight virus invasiveness by reinforcing the extracellular matrix. J Funct Foods. 2021;76:104318. Available from: https://linkinghub.elsevier.com/retrieve/pii/S1756464620305429.
100. Cook KC, Moreno JA, Jean Beltran PM, Cristea IM. Peroxisome Plasticity at the Virus–Host Interface. Trends Microbiol. 2019;27(11):906–14. Available from: https://linkinghub.elsevier.com/retrieve/pii/S0966842X19301611.
101. Di Cara F, Savary S, Kovacs WJ, Kim P, Rachubinski RA. The peroxisome: an up-and-coming organelle in immunometabolism. Trends Cell Biol. 2023;33(1):70–86. Available from: https://linkinghub.elsevier.com/retrieve/pii/S0962892422001404.
102. Wanders RJA, van Grunsven EG, Jansen GA. Lipid metabolism in peroxisomes: enzymology, functions and dysfunctions of the fatty acid α- and β-oxidation systems in humans. Biochem Soc Trans. 2000;28(2):141–9. Available from: https://portlandpress.com/biochemsoctrans/article/28/2/141/62960/Lipid-metabolism-in-peroxisomes-enzymology.
103. Jo DS, Park NY, Cho DH. Peroxisome quality control and dysregulated lipid metabolism in neurodegenerative diseases. Exp Mol Med. 2020;52(9):1486–95. Available from: https://www.nature.com/articles/s12276-020-00503-9.
104. Tang BL, Tan AEH, Lim LK, Lee SS, Low DYH, Hong W. Syntaxin 12, a Member of the Syntaxin Family Localized to the Endosome. J Biol Chem. 1998;273(12):6944–50. Available from: https://linkinghub.elsevier.com/retrieve/pii/S0021925818639717.
105. Kloc M, Uosef A, Wosik J, Kubiak JZ, Ghobrial RM. Virus interactions with the actin cytoskeleton—what we know and do not know about SARS-CoV-2. Arch Virol. 2022;167(3):737–49. Available from: https://link.springer.com/10.1007/s00705-022-05366-1.
106. Taylor MP, Koyuncu OO, Enquist LW. Subversion of the actin cytoskeleton during viral infection. Nat Rev Microbiol. 2011;9(6):427–39. Available from: https://www.nature.com/articles/nrmicro2574.
107. Bruder JT, Kovesdi I. Adenovirus infection stimulates the Raf/MAPK signaling pathway and induces interleukin-8 expression. J Virol. 1997;71(1):398–404. Available from: https://journals.asm.org/doi/10.1128/jvi.71.1.398-404.1997.

108. Hoving JC, Wilson GJ, Brown GD. Signalling C-Type lectin receptors, microbial recognition and immunity. Cell Microbiol. 2014;16(2):185–94. Available from: https://onlinelibrary.wiley.com/doi/10.1111/cmi.12249.
109. Coutermarsh-Ott S, Eden K, Allen IC. Beyond the inflammasome: regulatory NOD-like receptor modulation of the host immune response following virus exposure. J Gen Virol. 2016;97(4):825–38. Available from: https://www.microbiologyresearch.org/content/journal/jgv/10.1099/jgv.0.000401.
110. Rivas C, Aaronson SA, Munoz-Fontela C. Dual Role of p53 in Innate Antiviral Immunity. Viruses. 2010;2(1):298–313. Available from: https://www.mdpi.com/1999-4915/2/1/298.
111. Aloni-Grinstein R, Charni-Natan M, Solomon H, Rotter V. p53 and the Viral Connection: Back into the Future ‡. Cancers (Basel). 2018;10(6):178. Available from: http://www.mdpi.com/2072-6694/10/6/178.
112. Yuan D, Zhang Y, Liu W, He X, Chen W, Liu L, et al. Transcriptome profiling reveals transcriptional regulation of VISTA in T cell activation. Mol Immunol. 2023;157:101–11. Available from: https://linkinghub.elsevier.com/retrieve/pii/S0161589023000718.
113. Liu T, Zhang L, Joo D, Sun SC. NF-κB signaling in inflammation. Signal Transduct Target Ther. 2017 Jul 14;2(1):17023. Available from: https://www.nature.com/articles/sigtrans201723.
114. Zhao H, Granberg F, Pettersson U. How adenovirus strives to control cellular gene expression. Virology. 2007;363(2):357–75. Available from: https://linkinghub.elsevier.com/retrieve/pii/S0042682207001158.
115. Wang XP, Qi XF, Yang B, Chen SY, Wang JY. RNA-Seq analysis of duck embryo fibroblast cell gene expression during the early stage of egg drop syndrome virus infection. Poult Sci. 2019;98(1):404–12. Available from: https://linkinghub.elsevier.com/retrieve/pii/S0032579119303244.
116. Wang ZQ, Cefalu WT, Zhang XH, Yu Y, Qin J, Son L, et al. Human adenovirus type 36 enhances glucose uptake in diabetic and nondiabetic human skeletal muscle cells independent of insulin signaling. Diabetes. 2008;57(7):1805–13. Available from: http://www.ncbi.nlm.nih.gov/pubmed/18420488.
117. Bell GI, Kayano T, Buse JB, Burant CF, Takeda J, Lin D, et al. Molecular Biology of Mammalian Glucose Transporters. Diabetes Care. 1990;13(3):198–208. Available from: https://diabetesjournals.org/care/article/13/3/198/17045/Molecular-Biology-of-Mammalian-Glucose.
118. Fontaine KA, Camarda R, Lagunoff M. Vaccinia Virus Requires Glutamine but Not Glucose for Efficient Replication. Frueh K, editor. J Virol. 2014;88(8):4366–74. Available from: https://journals.asm.org/doi/10.1128/JVI.03134-13.
119. Collins MP, Forgac M. Regulation and function of V-ATPases in physiology and disease. Biochim Biophys Acta - Biomembr. 2020;1862(12):183341. Available from: https://linkinghub.elsevier.com/retrieve/pii/S0005273620301814.
120. Müller KH, Kainov DE, El Bakkouri K, Saelens X, De Brabander JK, Kittel C, et al. The proton translocation domain of cellular vacuolar ATPase provides a target for the treatment of influenza A virus infections. Br J Pharmacol. 2011;164(2):344–57. Available from: https://onlinelibrary.wiley.com/doi/10.1111/j.1476-5381.2011.01346.x.
121. Sahni A, Pei D. Bacterial Toxins Escape the Endosome by Inducing Vesicle Budding and Collapse. ACS Chem Biol. 2021;16(11):2415–22. Available from: https://pubs.acs.org/doi/10.1021/acschembio.1c00540.
122. Williams JM, Tsai B. Intracellular trafficking of bacterial toxins. Curr Opin Cell Biol. 2016;41:51–6. Available from: https://linkinghub.elsevier.com/retrieve/pii/S0955067416300692.
123. Zhang J, Zou Z, Huang K, Lin X, Chen H, Jin M. Insights into leghorn male hepatocellular cells response to fowl adenovirus serotype 4 infection by transcriptome analysis. Vet Microbiol. 2018 Feb;214:65–74. Available from: https://linkinghub.elsevier.com/retrieve/pii/S037811351731043X.
124. Walters RW, Freimuth P, Moninger TO, Ganske I, Zabner J, Welsh MJ. Adenovirus Fiber Disrupts CAR-Mediated Intercellular Adhesion Allowing Virus Escape. Cell. 2002;110(6):789–99. Available from: https://linkinghub.elsevier.com/retrieve/pii/S0092867402009121.

Publisher's Note